

Time Of Flight System for CLAS12

R. W. Gothe^a, G. V. Fedotov^a, E. Phelps^a, Iu. Skorodumina^a, Y. Tian^a, A. Trivedi^a, N. Tyler^a,

^a*University of South Carolina, Columbia, South Carolina 29208*

Abstract

In this paper the process of developing and testing of TOF system for CLAS12 is described. To speed up testing process new so-called “6-bar” method of time resolution determination using cosmic rays is developed. With new measuring procedure the world record time resolution for given scintillator length is achieved.

Keywords: TOF, Nuclear physics experiment

1. 12-GeV upgrade and CLAS12 overview

Note:

Detector-based rather than physics-based.

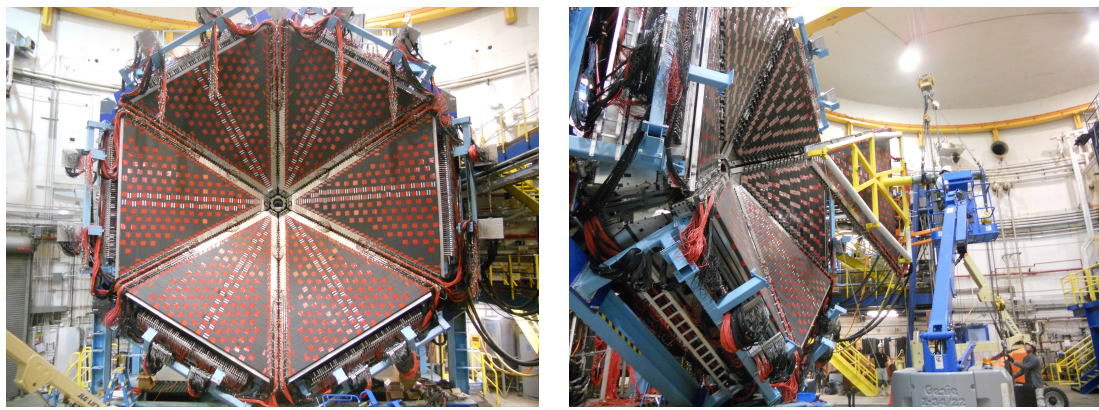
Condense content of other CLAS12 publications.

Highlight specific requirement of each detector subsystem for particle reconstruction in different kinematic regimes.

Segue into next section FTOF12

Important figures:

complete detector → FTOF12 at that level



(a) FTOF panels installed in Hall-B.

(b) FTOF installation process.

Figure 1

2. FTOF12 requirements and high-level design

Important figures:

particle separation curves on t vs. p assuming 4separation (pK , $K\pi$, $p\pi$). print quality version of some combination of these:

resolution curves on time resolution vs. counter length (old, new, combined)

resolution curves on time resolution vs. counter length per scintillator material (per advertised attenuation lengths)

CLAS12 geometry \rightarrow FTOF12 geometry (zoom in, light guides and PMT form-factors) stray B-field map (or just state upper bound)

stray B-field map (or just state upper bound)

The time-of-flight subsystem of the CLAS detector in Hall B was designed to allow separation of pions and kaons in the kinematic range accessible with a 6-*GeV* electron beam by providing time resolutions from 90 *ps* to 160 *ps* at the forward angles, where the most energetic particles are detected. [1] To reliably separate p , π , and K in the kinematic range accessible with the proposed 11-*GeV* beam of the CEBAF upgrade, the FTOF detector must achieve a resolution of 80 *ps* [2] as illustrated in Fig. 5. This assumes a 4σ time difference between two particles, thus allowing for identification of a signal in the presence of other particles with a ten-fold higher rate.

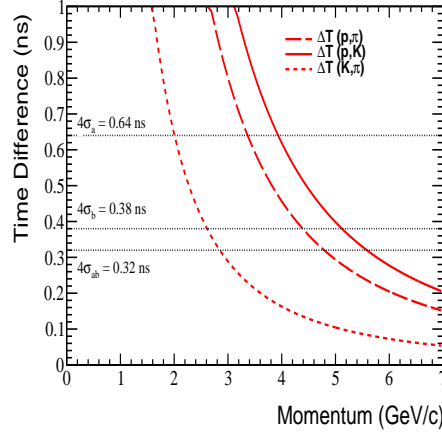


Figure 2: The three curves indicate the time differences, Δt , between p/π , p/K , and π/K over the 650 cm path length from the target to Panel 1B.

As in the current 6-*GeV* FTOF detector (Panel 1A), each counter of the additional 12-*GeV* FTOF (Panel 1B) is composed of a long rectangular plastic scintillator with two cylindrical PMTs, one on each end, directly attached without light guides. The scintillator lengths are tightly constrained by the established six-panel FTOF geometry and the requirement that the new panels do not restrict the CLAS12 acceptance as defined by the other detector components, but the thickness

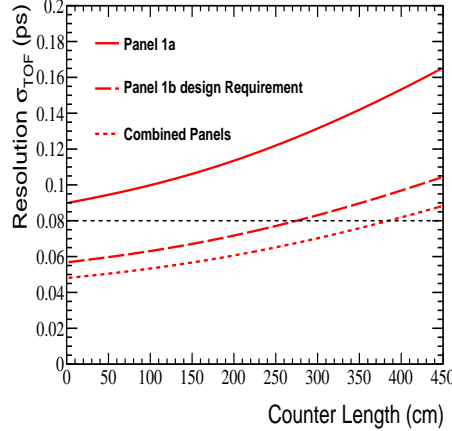


Figure 3: Solid line, the measured and parameterized average standard deviation $\overline{\sigma_{ToF}}$ time resolution of the existing panel-1a counters (15 cm wide, 5 cm thick) fit with an assumed intrinsic electronic resolution of 40 ps [?]. Scaling the parametrization by $\sqrt{\frac{2}{5}}$ leads to the Long dashed line representing the new panel-1b counters (6cm wide, 6cm thick) and short dashed line the combined panel-1a and panel-1b counters time resolution. The black straight short dashed line is the design requiement for combined time resolution

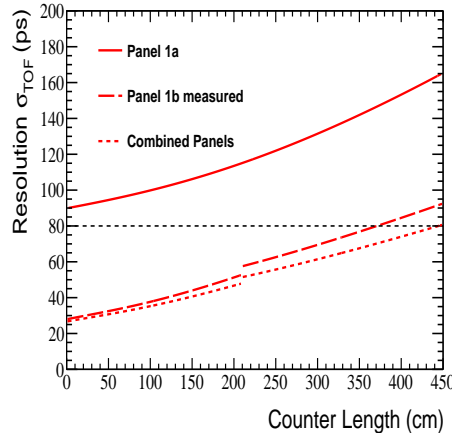
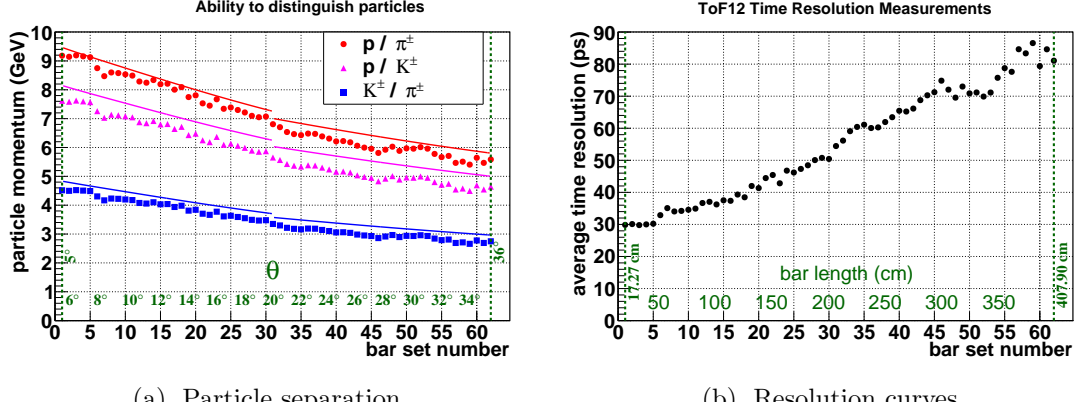


Figure 4: Solid line, the measured and parameterized average standard deviation $\overline{\sigma_{ToF}}$ time resolution of the existing panel-1a counters (15 cm wide, 5 cm thick) fit with an assumed intrinsic electronic resolution of 40 ps [?]. USC measured and parameterized average standard deviation time resolution of panel-1b leads to the Long dashed line representing the new panel-1b counters (6cm wide, 6cm thick) and short dashed line the combined panel-1a and panel-1b counters time resolution. The black straight short dashed line is the design requiement for combined time resolution

and width, $6\text{ cm} \times 6\text{ cm}$, are selected to optimize photon statistics, geometric matching with the photocathodes, and closest possible stacking. Compared to the Panel-1A $5\text{ cm} \times 15\text{ cm}$ FTOF scintillators, the $6\text{ cm} \times 6\text{ cm}$ scintillators increase the number of photons produced by a factor of $6/5$; the increased ratio of photocathode area to scintillator exit window area increases the number of photons that reach the photocathode by at least a factor of $25/12$. Thus, disregarding that the area ratio factor acts on the number of photons after light attenuation, the Panel-1B scintil-



(a) Particle separation.

(b) Resolution curves.

Figure 5: (a) Maximum momentum up to which particles can be separated as function of bar set number or polar angle theta. Calculations were made in assumption of 700-cm path length from the target to Panel 1B. [2]. Various symbols represent different particle pairs: red circles - p/π^\pm , purple triangles - p/K^\pm , and blue squares - K^\pm/π^\pm . Curves represent combined ability of Panel 1A and Panel 1B to separate particles over momentum. Colors of the curves correspond to the colors of symbols. (b) Time resolution averaged over six same length individual bars as function of bar set number or bar length for measurements performed at USC.

lator geometry increases the number of photons reaching the photocathode by a factor of about $5/2$ and, therefore, improves the resolution by a factor of $\sqrt{2/5}$, neglecting the resolution of any contributions that are independent of light level.

With a resolution of better than 150 ps for the longest counters of Panel 1A, the Panel-1B counters must achieve resolutions better than 95 ps for the combined resolution goal of 80 ps to be reached (Fig. 5). Preliminary prototype results exceed this requirement.

2.0.1. Source method

One of the methods that can be used to determine counter resolution is so called "source" or "coordinate method" (see CLAS-NOTE 2004-016 [3]) that is based on the fact that the light flash coordinate and arrival times of signals in two PMTs are correlated. In this method radioactive small Sr-90 β -source is placed in various positions along the bar in order to measure position-specific resolution.

For given project this method is highly inappropriate for two main reasons: (a) large number of counters (372) with length up to four meters leads to huge amount of manual measurements; (b) the Sr-90 events are not representative neither in penetration depth nor photon statistics, since energy of β -particles from the source is in order of MeV, while particles that will be measured in CLAS12 have energy order of GeV.

Thus this method was used for initial electronic and selected individual counters test only.

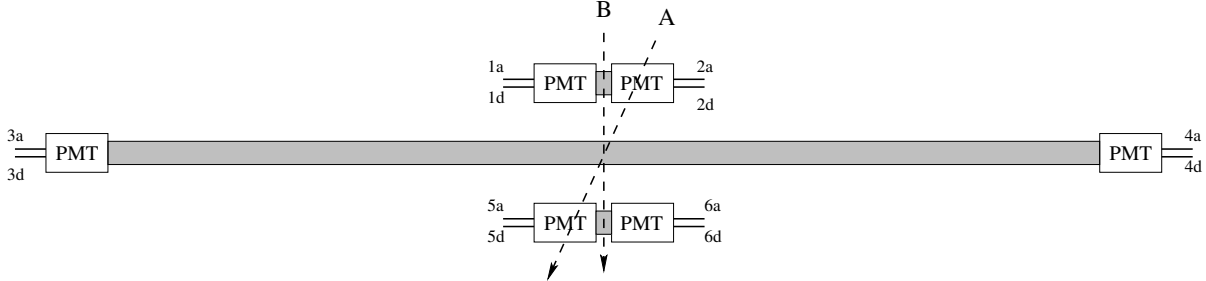


Figure 6: In the thin scintillator cosmic ray method, 5mm-thin scintillators are placed above and below the counter to be tested so that the position of cosmic ray events on the middle counter is fixed. The TDC difference between left and right PMTs on the middle counter is then used to determine the counter's resolution. Only vertical tracks such as B survive, when signals in six PMTs are in coincidence.

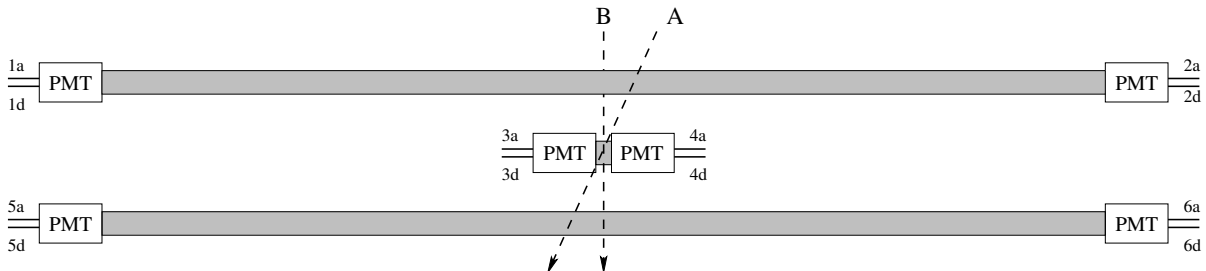


Figure 7: This variant of the reference counter method does not physically restrict particles to pass through vertically (path B), because particles along path A also triggers all six PMTs. However, paths such as A are further reduced by cutting away middle-bar low ADC values, which correspond generally to particles traveling through less than the 5-cm vertical extent of the middle scintillator.

2.0.2. Thin scintillator cosmic ray method

Another method of counter resolution determination is so-called "thin scintillator cosmic rays method" that uses two thin scintillators to effectively collimate cosmic rays trajectories to perpendicularly traverse the counter at a fixed position, as shown in Fig. 6. In this method time information from top and bottom counters is not needed. In order to fix track position signal coincidence in six PMTs is required. This method was tested using five millimeters thin scintillators and it turned out that event rate is extremely low. Moreover, like in source method described in Sec. 2.0.1 huge amount of manual measurements is needed.

In order to increase event rate this method can be modified as shown in Fig. 7. In that case one thin scintillator ten times thicker than in previous setup is positioned between two longer scintillators achieving a partial collimation. Since non vertical tracks shown as A on Fig. 7 pass only part of the middle scintillator height, amplitudes of their signals are lower then from the vertical tracks shown by B on Fig. 7. So the positions on top and bottom scintillators are further restricted by cutting away low ADC events on the middle bar. But it turned out that this procedure does not sufficiently increase event rate and does not allow to get rid of the multiple manual measurements.

Both described variants of thin scintillator cosmic rays method can be transformed into so-called "reference counter method", in which thin scintillator counters need to be replaced by reference counters with known resolutions. In that case one should use TDC information from reference counters and vertical tracks selection is not needed anymore that lead to the higher event rate. Then it becomes possible for setup like shown on Fig. 6 to derive the resolution of tested counter through the resolutions of reference counters, and for setup like shown on Fig. 7 to derive the combined resolution of two tested counters through the resolution of the known one.

In case of the need to test many similar counters it is natural to build setup from the three counters of the same lenght and to extract their combined resolution. These modifications lead to the three bar cosmic rays method described in Sec. 3.1

3. Six Bar Cosmic-Ray Method

The six bar cosmic-ray method is a generalization and improvement of the three bar cosmic-ray method facilitating individual counter resolution measurements. As such, it is necessary to recapitulate the three bar cosmic-ray method prior to presenting the six bar cosmic-ray method.

3.1. Three Bar Cosmic-Ray Method

The three bar cosmic-ray method (hereafter known as the three bar method) allows the determination of the time resolution of a counter given two counters with known time resolutions. A counter here is a scintillator with photomultiplier tubes (PMTs) attached at each end. The three bar cosmic-ray method proceeds by stacking the three counters vertically with equal spacing between adjacent counters and each counter being parallel to the other two.

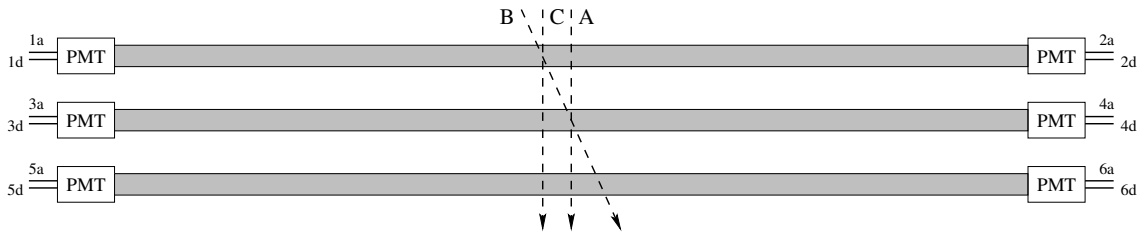


Figure 8: In the three bar method, cosmic-ray particles are required to pass through all three counters. A, B, and C denote possible particle paths through the three counters.

Cosmic-ray particles will interact with the counters at random. If only those events in which all three counters detected a cosmic-ray particle are considered, then the geometry of the setup allows the unknown resolution to be determined. The detected cosmic-ray particles are assumed to have high enough energy so that the paths they take are straight to good approximation (a good assumption in practice). Since the counters are arranged to be parallel with equal spacing, and since the particle travels with fixed velocity, the time taken to travel between any pair of adjacent counters is the same.

The interacting cosmic-ray particle causes each PMT to signal; these are sent to a time-to-digital converter (TDC) and reported as the interaction time of the scintillation light with the PMT. One of the six PMTs is chosen to provide the reference time for the event t_{ref} . The reference time is subtracted from the raw time reported from the TDC for each PMT since the raw TDC reported times have arbitrary offsets. Therefore the reference-subtracted timing for each PMT is given by $t = t_{\text{raw}} - t_{ref}$.

The time that the cosmic-ray particle interacts with the i th scintillator is given by

$$t'_i = \frac{t_{iL} + t_{iR}}{2} - \frac{L}{2v} \quad (3.1)$$

where t_{iL} and t_{iR} are the left and right PMTs for the scintillator respectively, L is the length of the scintillator, and v is the effective speed of light of the scintillator.

However, since the counters have the same geometry and are made of the same material, the counter term $-\frac{L}{2v}$ is the same for each counter and can be subtracted from each counter interaction time to yield

$$t_i = t'_i + \frac{L}{2v} = \frac{t_{iL} + t_{iR}}{2}. \quad (3.2)$$

The counter interaction times for each of the three counters should be given by:

$$t_t = \tau + \varepsilon_t, \quad (3.3)$$

$$t_m = \tau + \varepsilon_m + \delta, \quad (3.4)$$

and

$$t_b = \tau + \varepsilon_b + 2\delta, \quad (3.5)$$

where the t_i are the measured interaction times reported by the electronics for each counter (top, middle, and bottom), τ is the actual time at which the cosmic-ray particle interacts with the top counter, the ε_i are all the error contributions to the measured time including those due to the electronics as well as the intrinsic random contributions, and δ is the time it takes the cosmic-ray particle to move between adjacent counters. As noted above, this time δ is the same for any pair of adjacent counters due to equal spacing and the straight trajectory of the cosmic-ray particle.

Note that the quantity

$$T = \frac{t_t + t_b}{2} - t_m = \frac{\varepsilon_t + \varepsilon_b}{2} - \varepsilon_m \quad (3.6)$$

does not depend on τ or δ . Since the resolution of the readout electronics is typically small compared to the statistical uncertainty in T , the statistical uncertainty in T only depends on the resolutions of the three counters:

$$\sigma_T^2 = (\sigma_{\varepsilon_t}^2 + \sigma_{\varepsilon_b}^2)/4 + \sigma_{\varepsilon_m}^2 \quad (3.7)$$

where the σ_{ε_i} are the statistical resolutions of the individual counters. The assumption of identical counters, $\forall i \sigma_{\varepsilon_i} = \sigma_\varepsilon$, implies finally that

$$\sigma_T^2 = \frac{3}{2}\sigma_\varepsilon^2 \quad (3.8)$$

or, rearranging,

$$\sigma_\varepsilon = \sqrt{\frac{2}{3}}\sigma_T \quad (3.9)$$

3.2. The Six Bar Cosmic-Ray Method

The six bar method cosmic-ray method (hereafter known as the six bar method) consists of six simultaneous three bar measurements. The system of equations for the counter resolutions that arises due to Gaussian error propagation is then solved for the individual counter resolutions.

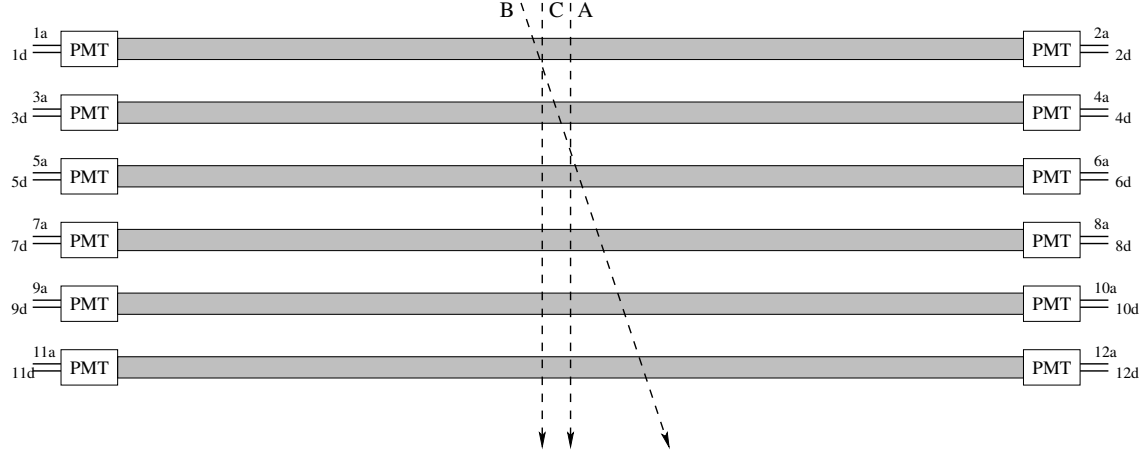


Figure 9: Depiction of six bar method setup.

Analogous to the three counters in the three bar method, six identical-length counters are stacked vertically and equally-spaced, and events are selected according to the requirement that the cosmic-ray particle was detected by all six counters. Labeling the counters 1 through 6, starting with the top counter, and using the notation (top, middle, bottom) to represent the counters involved in each three bar measurement, the three-bar measurements performed are: (1,2,3), (2,3,4), (3,4,5), (4,5,6), (1,3,5), and (2,4,6). These are the only possible combinations of three counters in which the spacing between adjacent counters is the same.

Six Bar Combinations

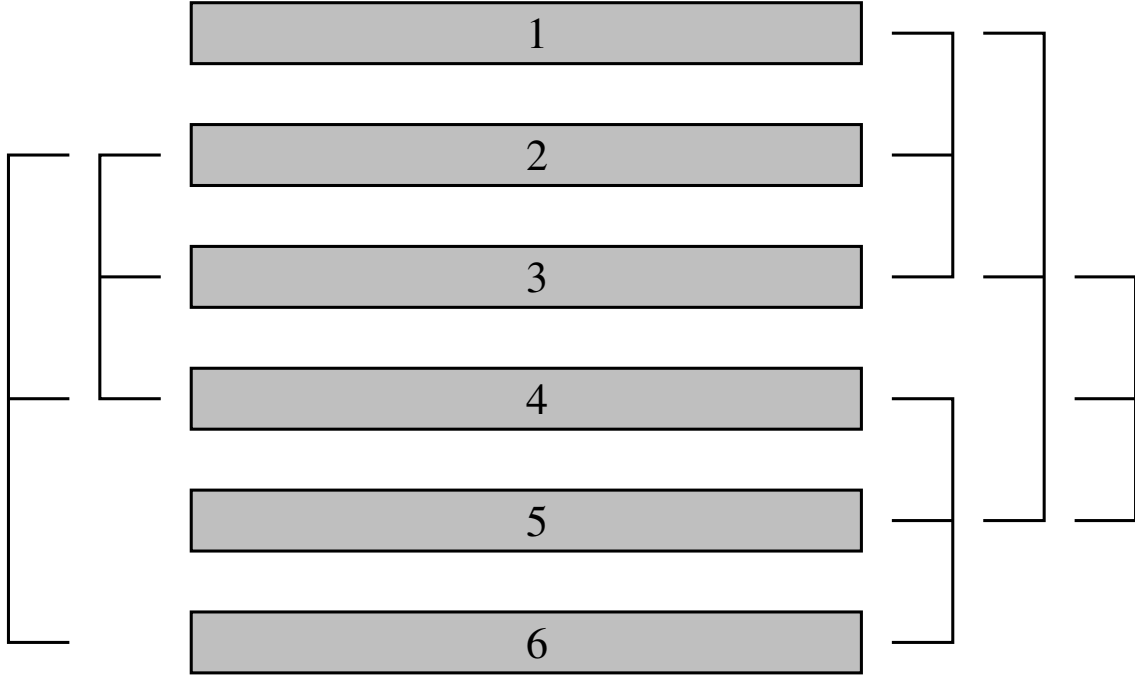


Figure 10: Depiction of which three bar combinations are selected for the six bar method.

Using t_n for the cosmic-ray interaction times through the n th counter, the three-bar method observables for each of the six combinations of three counters are given by:

$$T_{(1,2,3)} = (t_1 + t_3)/2 - t_2, \quad (3.10)$$

$$T_{(2,3,4)} = (t_2 + t_4)/2 - t_3, \quad (3.11)$$

$$T_{(3,4,5)} = (t_3 + t_5)/2 - t_4, \quad (3.12)$$

$$T_{(4,5,6)} = (t_4 + t_6)/2 - t_5, \quad (3.13)$$

$$T_{(1,3,5)} = (t_1 + t_5)/2 - t_3, \quad (3.14)$$

$$T_{(2,4,6)} = (t_2 + t_6)/2 - t_4. \quad (3.15)$$

Applying error propagation to the above equations, this system of equations for the counter resolutions follows:

$$\begin{cases} \sigma_{T_{(1,2,3)}}^2 = (\sigma_1^2 + \sigma_3^2)/4 + \sigma_2^2 \\ \sigma_{T_{(2,3,4)}}^2 = (\sigma_2^2 + \sigma_4^2)/4 + \sigma_3^2 \\ \sigma_{T_{(3,4,5)}}^2 = (\sigma_3^2 + \sigma_5^2)/4 + \sigma_4^2 \\ \sigma_{T_{(4,5,6)}}^2 = (\sigma_4^2 + \sigma_6^2)/4 + \sigma_5^2 \\ \sigma_{T_{(1,3,5)}}^2 = (\sigma_1^2 + \sigma_5^2)/4 + \sigma_3^2 \\ \sigma_{T_{(2,4,6)}}^2 = (\sigma_2^2 + \sigma_6^2)/4 + \sigma_4^2 \end{cases} \quad (3.16)$$

Written in matrix form, the system of equations is:

$$\begin{bmatrix} \sigma_{T_{(1,2,3)}}^2 \\ \sigma_{T_{(2,3,4)}}^2 \\ \sigma_{T_{(3,4,5)}}^2 \\ \sigma_{T_{(4,5,6)}}^2 \\ \sigma_{T_{(1,3,5)}}^2 \\ \sigma_{T_{(2,4,6)}}^2 \end{bmatrix} = \begin{bmatrix} \frac{1}{4} & 1 & \frac{1}{4} & 0 & 0 & 0 \\ 0 & \frac{1}{4} & 1 & \frac{1}{4} & 0 & 0 \\ 0 & 0 & \frac{1}{4} & 1 & \frac{1}{4} & 0 \\ 0 & 0 & 0 & \frac{1}{4} & 1 & \frac{1}{4} \\ \frac{1}{4} & 0 & 1 & 0 & \frac{1}{4} & 0 \\ 0 & \frac{1}{4} & 0 & 1 & 0 & \frac{1}{4} \end{bmatrix} \begin{bmatrix} \sigma_1^2 \\ \sigma_2^2 \\ \sigma_3^2 \\ \sigma_4^2 \\ \sigma_5^2 \\ \sigma_6^2 \end{bmatrix} \quad (3.17)$$

Since the determinant of the coefficient matrix is non-zero (81/1024), the system is independent and can be solved to yield the σ_i^2 by one of the many available techniques to solve a linear system of equations.

3.3. Refinement of the Six Bar Method

The method as stated above suffers from a fundamental asymmetry in the way the counters are used in the calculations (as shown in the table below): The inner two counters are each involved in four of the T_k , whereas the next outer two are only necessary for three each and the outer most are only used in two of the T_k ; this causes some counters to have a stronger influence on the computed counter resolutions than others. In practice this results in large fluctuations in the computed counter resolutions, but can be helped with a slight modification to the method.

| Counter | # of Dependent T_k | Dependent Combinations |
|---------|----------------------|------------------------------------|
| 1 | 2 | (1,2,3), (1,3,5) |
| 2 | 3 | (1,2,3), (2,3,4),(2,4,6) |
| 3 | 4 | (1,2,3), (2,3,4), (3,4,5), (1,3,5) |
| 4 | 4 | (2,3,4), (3,4,5), (4,5,6), (2,4,6) |
| 5 | 3 | (3,4,5), (4,5,6), (1,3,5) |
| 6 | 2 | (4,5,6), (2,4,6) |

To remedy this, two consecutive 6-bar measurements are run instead of one, with the second measurement having the counters stacked in a different order (known as the *complementary ordering*). The order was selected to make the number of equations containing each counter resolution the same, and is described by the permutation, from top to bottom, (3,2,1,6,5,4).

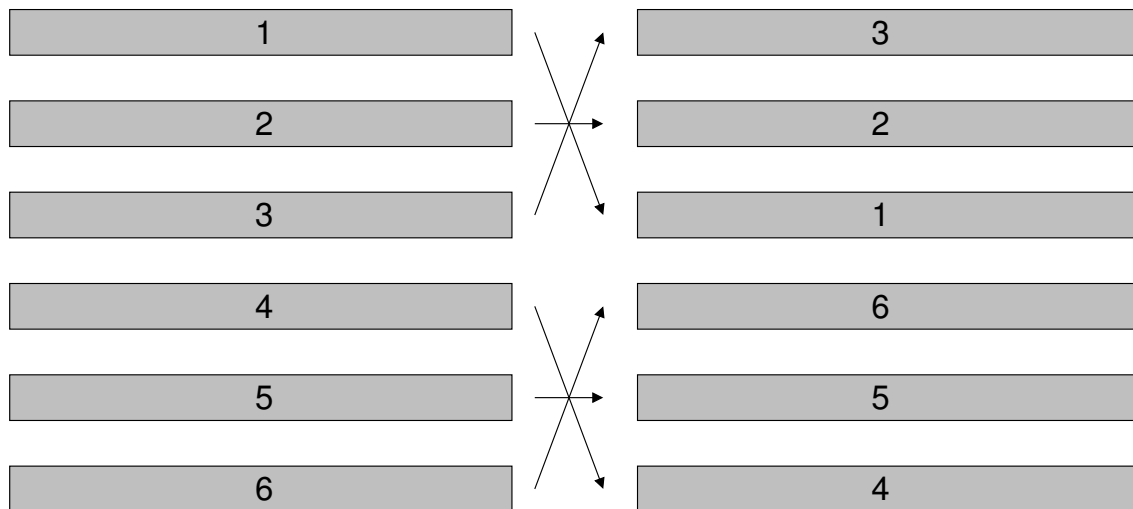


Figure 11: Rearrangement of the six counters for the complementary measurement.

The additional three bar observables are

$$T_{(3,2,1)} = (t_3 + t_1)/2 - t_2, \quad (3.18)$$

$$T_{(2,1,6)} = (t_2 + t_6)/2 - t_1, \quad (3.19)$$

$$T_{(1,6,5)} = (t_1 + t_5)/2 - t_6, \quad (3.20)$$

$$T_{(6,5,4)} = (t_6 + t_4)/2 - t_5, \quad (3.21)$$

$$T_{(3,1,5)} = (t_3 + t_5)/2 - t_1, \quad (3.22)$$

$$T_{(2,6,4)} = (t_2 + t_4)/2 - t_6, \quad (3.23)$$

leading to the following over-constrained system of equations for the individual counter resolutions,

$$\left\{ \begin{array}{l} \sigma_{T_{(1,2,3)}}^2 = (\sigma_1^2 + \sigma_3^2)/4 + \sigma_2^2 \\ \sigma_{T_{(2,3,4)}}^2 = (\sigma_2^2 + \sigma_4^2)/4 + \sigma_3^2 \\ \sigma_{T_{(3,4,5)}}^2 = (\sigma_3^2 + \sigma_5^2)/4 + \sigma_4^2 \\ \sigma_{T_{(4,5,6)}}^2 = (\sigma_4^2 + \sigma_6^2)/4 + \sigma_5^2 \\ \sigma_{T_{(1,3,5)}}^2 = (\sigma_1^2 + \sigma_5^2)/4 + \sigma_3^2 \\ \sigma_{T_{(2,4,6)}}^2 = (\sigma_2^2 + \sigma_6^2)/4 + \sigma_4^2 \\ \sigma_{T_{(3,2,1)}}^2 = (\sigma_3^2 + \sigma_1^2)/4 - \sigma_2^2 \\ \sigma_{T_{(2,1,6)}}^2 = (\sigma_2^2 + \sigma_6^2)/4 - \sigma_1^2 \\ \sigma_{T_{(1,6,5)}}^2 = (\sigma_1^2 + \sigma_5^2)/4 - \sigma_6^2 \\ \sigma_{T_{(6,5,4)}}^2 = (\sigma_6^2 + \sigma_4^2)/4 - \sigma_5^2 \\ \sigma_{T_{(3,1,5)}}^2 = (\sigma_3^2 + \sigma_5^2)/4 - \sigma_1^2 \\ \sigma_{T_{(2,6,4)}}^2 = (\sigma_2^2 + \sigma_4^2)/4 - \sigma_6^2 \end{array} \right. \quad (3.24)$$

and in matrix form,

$$\begin{bmatrix}
\sigma_{T_{(1,2,3)}}^2 \\
\sigma_{T_{(2,3,4)}}^2 \\
\sigma_{T_{(3,4,5)}}^2 \\
\sigma_{T_{(4,5,6)}}^2 \\
\sigma_{T_{(1,3,5)}}^2 \\
\sigma_{T_{(2,4,6)}}^2 \\
\sigma_{T_{(3,2,1)}}^2 \\
\sigma_{T_{(2,1,6)}}^2 \\
\sigma_{T_{(1,6,5)}}^2 \\
\sigma_{T_{(6,5,4)}}^2 \\
\sigma_{T_{(3,1,5)}}^2 \\
\sigma_{T_{(2,6,4)}}^2
\end{bmatrix} = \begin{bmatrix}
\frac{1}{4} & 1 & \frac{1}{4} & 0 & 0 & 0 \\
0 & \frac{1}{4} & 1 & \frac{1}{4} & 0 & 0 \\
0 & 0 & \frac{1}{4} & 1 & \frac{1}{4} & 0 \\
0 & 0 & 0 & \frac{1}{4} & 1 & \frac{1}{4} \\
\frac{1}{4} & 0 & 1 & 0 & \frac{1}{4} & 0 \\
0 & \frac{1}{4} & 0 & 1 & 0 & \frac{1}{4} \\
\frac{1}{4} & 1 & \frac{1}{4} & 0 & 0 & 0 \\
1 & \frac{1}{4} & 0 & 0 & 0 & \frac{1}{4} \\
\frac{1}{4} & 0 & 0 & 0 & \frac{1}{4} & 1 \\
0 & 0 & 0 & \frac{1}{4} & 1 & \frac{1}{4} \\
1 & 0 & \frac{1}{4} & 0 & \frac{1}{4} & 0 \\
0 & \frac{1}{4} & 0 & \frac{1}{4} & 0 & 1
\end{bmatrix} \begin{bmatrix}
\sigma_1^2 \\
\sigma_2^2 \\
\sigma_3^2 \\
\sigma_4^2 \\
\sigma_5^2 \\
\sigma_6^2
\end{bmatrix}, \quad (3.25)$$

or just

$$\vec{T} = \hat{A}\vec{\sigma}. \quad (3.26)$$

In the combined over-constrained system of equations, each counter resolution occurs in six equations. This modification makes the method noticeably more stable when computing the individual counter resolutions. As the new system of equations is over-constrained, the best estimator for the solution to the system is given by the method of linear least-squares. Linear least-squares consists of solving the following equation for $\vec{\sigma}$:

$$(\hat{A}^T \hat{A})\vec{\sigma} = \hat{A}^T \vec{T}. \quad (3.27)$$

3.4. Electronics

The primary electronic subsystem components relevant to FTOF12 time resolution are discriminators, time-to-digital converters (TDC), and charge-to-digital converters (QDC). Each anode PMT pulse of sufficient amplitude generates a logic signal by way of a discriminator, and the logic signal's time of arrival is measured by a TDC. In parallel, the corresponding dynode PMT pulse is integrated by a QDC. In the case of FTOF12's fixed-risetime PMT signals, the time required for the incoming signal to reach the discriminator threshold (timewalk) can be subtracted according to the signal size, which is proportional to the corresponding QDC value. The TDC sets the fundamental lower limit on the time resolution measurement, the discriminator introduces time variations primarily through timewalk, and the QDC provides information that allows for time-walk correction. Accordingly, the properties of each of these components are crucial to achieving optimal time resolution.

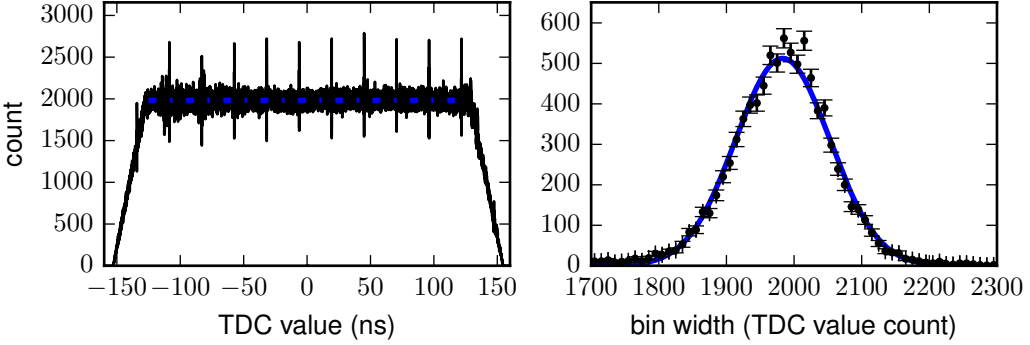


Figure 12: The DNL histogram (left) deviates from an ideal uniform distribution, indicated by the dotted line, with a standard deviation of 70 counts (right), so the relative nonlinearity is $\frac{70}{1983} = 3.5\%$. After compensating for the statistical contribution of $\frac{\sqrt{1983}}{1983} = 2.2\%$, the relative DNL is 2.7%. The sloped edges result from the 25 ns variability in the V1290N’s timing window with respect to the trigger. The periodic needles, again at 25 ns intervals, result from INL compensation on the TDC chip level.[4] The additional interference at TDC value 0 results from crosstalk between the two signals.

3.4.1. TDC testing

Important figures:

integral nonlinearity (INL) – cable delay plots

differential nonlinearity (DNL) – white histogram, channel width distribution

intrinsic time resolution

dithering mode on versus off

The properties of the TDC determine the most basic unit of time resolution. Resolution, differential nonlinearity (DNL), and integral nonlinearity (INL), were measured for common-start CAMAC modules (Phillips Scientific PS7186 and Caen C414) and a newer pipeline VME module (Caen V1290N). Neither CAMAC module met the manufacturer’s specifications, but the Caen VME module V1290N performed acceptably, which was one factor in the choice to use VME during our prototype development. Ultimately, however, the pipeline class of TDC is required for a more basic reason: it allows for the decoupling of the coincidence trigger from the timing trigger, which removes all electronic logic system contributions other than the discriminator from the time resolution.

In order to determine the DNL profile of each module, a random start signal and periodic stop signal are fed to the TDC. The stop signal arrives at the TDC in any fixed-width time interval with equal probability. Thus, after a large number of events, a uniform distribution of counts per time interval (bin) is expected in the ideal case. Deviations from the ideal result minus statistical noise reflect the TDC’s DNL.

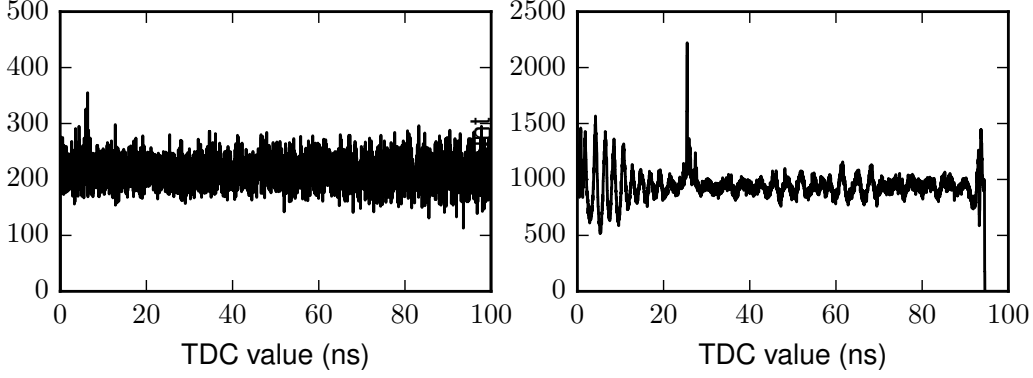


Figure 13: DNL histograms for the Phillips Scientific 7186 (left) and the Caen 414 (right), compared with that of the Caen V1290N (Fig. 12, left), illustrate different nonlinearity signatures. The PS7186 and C414 are 12-bit CAMAC modules with limited ranges. The entire 100 ns range (12-bit) is usable in the PS7186, but the high nonlinearity below bin 1100 of the C414 restricts the usable range to only about 60 ns .

| Model | DNL $_{\sigma}$ | DNL $_{max}$ | Range(ns) | Offset(ns) | Bin Size(ps) | Resolution(ps) |
|--------|-----------------|--------------|-----------|------------|--------------|----------------|
| PS7186 | 9.4% | 48.9% | 100 | 18-21 | 24.98 | 19.0 |
| C414 | 6.5% | 135.6% | 72 | 0-5 | 25.11 | 17.5 |
| V1290N | 2.7% | 41.1% | N/A | N/A | 24.75 | 32.5 |

Table 1: TDC Summary.

A radioactive source of Sr-90, placed on a counter, provides the random signals, which are converted to NIM logic signals by a leading edge discriminator (Phillips Scientific 705) for timing. In parallel, a timing unit (Phillips Scientific 794) provides logic pulses with a period greater than the TDC full range for the common-start CAMAC TDCs and a period of 200 ns for the pipeline VME TDC. The random signal serves as the reference signal, and the periodic signal, sent to all channels via a logic fan in/out (LeCroy 429A), serves as the channel-specific stop. A TDC value distribution and its corresponding bin-width distribution are histogrammed in Fig. 12, and for comparison, the DNL histograms of PS7186 and C414 are illustrated in Fig. 13.

Calibration of the TDCs was accomplished by applying variable, oscilloscope-measured cable delays in 5 ns increments. Figure 14 demonstrates the calibration procedure where, in the illustrated case of the Caen C414, the average bin width is 25.11 ps with an offset of 2.8 ns . Each 5 ns -interval peak includes 1000 entries and has a width corresponding to 0.6 bins $< \sigma <$ 0.8 bins. Results for each TDC are tabulated in Table 1.



Figure 14: Typical TDC calibration results illustrated for the Caen C414. Two copies of the same signal are used as start and stop times, with the latter being delayed with measured cable lengths in 5 ns increments (top). The typical peak width corresponds to $\sigma = 0.7\text{ bins}$. The mean TDC value of each peak is plotted with its corresponding measured delay (bottom) to get the TDC sensitivity and offset (parameters p_1 and p_0 , respectively).

3.4.2. QDC testing

Note: variable offset (motivating external DC offset)

dynamic range

DNL/INL (*?)

For the purpose of time resolution measurements, the QDC is only used in correcting for signal time of arrival, so calibrating the QDC values to an absolute energy scale of energy deposited is unnecessary. However, identifying the module's ground and the system charge offset (the zero) is crucial. For the prototype testing, the Caen V792N QDC[5] (integrating QDC) was tested and calibrated such that the zero was in an acceptable range using a combination of the module's software-adjustable pedestal and an externally applied DC offset. To identify the full range of the QDC's pedestal, a fixed-width integration gate ($T_{gate} = 100 \text{ ns}$) and measured DC offsets are applied to a ground signal and integrated for various pedestal settings (Fig. 15).

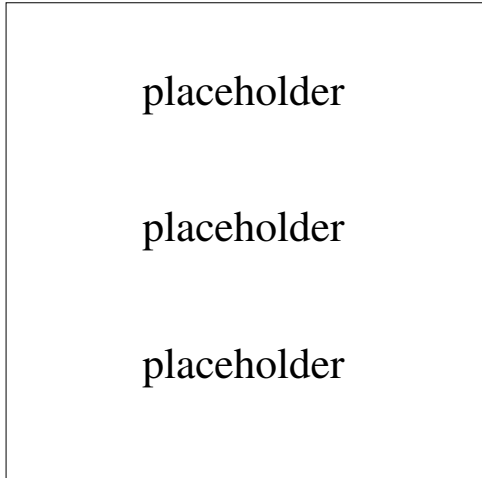


Figure 15: A fixed-width integration gate, T_{gate} , and variable DC offsets, V_1-V_7 are used to calibrate the QDC, including sensitivity and pedestal measurements.

Figure 16 illustrates the QDC distribution when the pedestal is set to 63 and an external DC offset of -22.55 mV is applied. Combining such results for various DC offsets, the relationship between the DC offset and QDC value is determined (see Fig. 17(a)). The y -intercept of the best-fit line indicates the QDC's virtual ground, its pedestal current, with respect to which it integrates incoming signals. Finally, the module's pedestal settings are compared to the corresponding virtual ground values to determine the full range of the adjustable intrinsic pedestal, as shown in Fig. 17(b).

The sensitivity of the QDC is determined from Fig. 17(a), where the best-fit line is cast in terms of charge rather than DC offset as in equation (3.28), where Q corresponds to total charge,

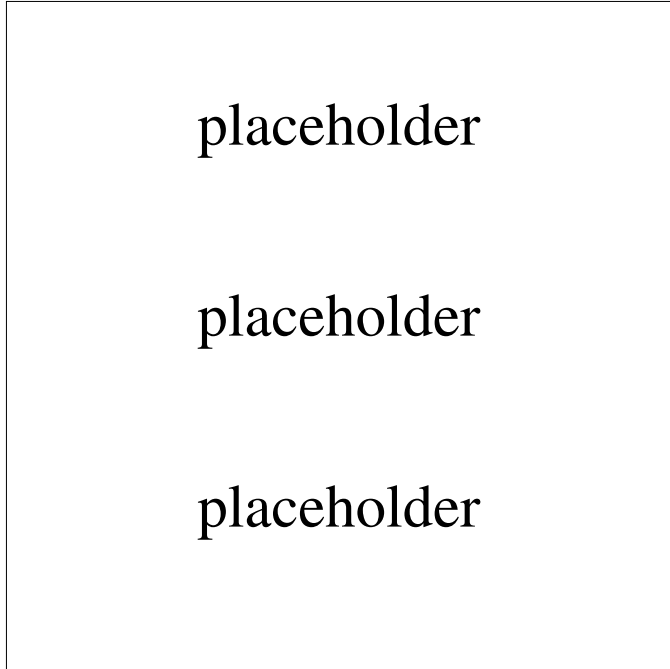
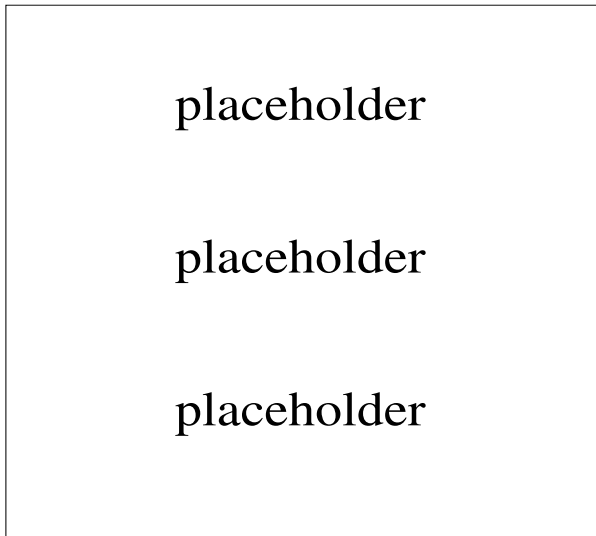


Figure 16: An QDC distribution corresponding to a -22.55 mV offset integrated over 100 ns .

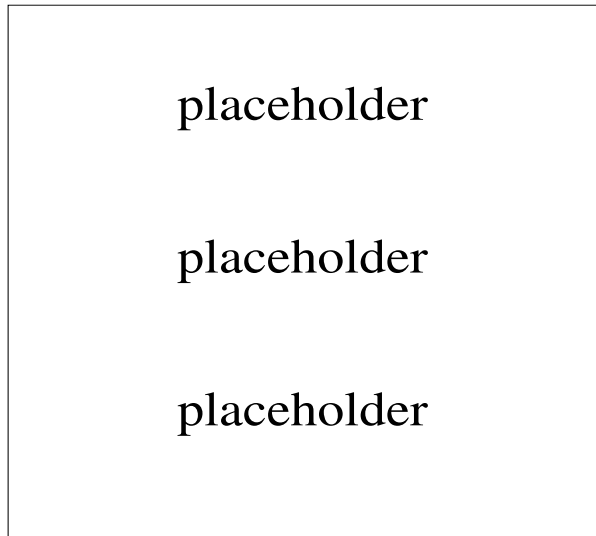
x to QDC value (bin), and R to resistance (50Ω).

$$Q = \left(-4.606 \frac{\text{mV}}{\text{bin}} x - 0.0542 \text{ mV} \right) \left(\frac{T_{gate}}{R} \right) = -9.2 \frac{\text{pC}}{\text{bin}} x - 0.11 \text{ pC} \quad (3.28)$$

Accordingly, the V792N's sensitivity of $9.2 \frac{\text{pC}}{\text{bin}}$ is consistent with the documented sensitivity of $10 \frac{\text{pC}}{\text{bin}}$.



(a) DC offset versus QDC.



(b) Pedestal setting versus virtual ground.

Figure 17: (a) For the adjustable pedestal setting of 63, the module has a virtual ground of -4.6 mV as determined by the QDC zero-crossing. (b) This zero-crossing varies from $\approx 0\text{ mV}$ to $\approx -6\text{ mV}$, so even in this case, an external DC offset is required to push the overall system offset into the active QDC range.

3.4.3. Discriminator testing

*Note: constant fraction discriminator (cfd) delay optimization
leading edge discriminator (led) threshold optimization
cfd vs. led vs. tw-corrected led (*?)*

Discriminators generate logic signals whenever incoming analog signals rise above a preset threshold voltage. Two classes of discriminators are common: constant fraction discriminators (CFD) and leading edge discriminators (LED). CFDs are designed to correct for timewalk by triggering on the sum of the incoming signal and a delayed, attenuated, and inverted duplicate. LEDs trigger directly on the incoming signal. Properly tuned CFDs were sufficient for previous time-of-flight applications, but FTOF12 is sensitive to an additional QDC-based timewalk correction to CFD-triggered signals. Since these additional timewalk corrections would be required in either case, the simpler and less expensive LEDs were used.

In the case of LEDs, the threshold voltage must be optimized to minimize background, maximize good signal acceptance, and reduce time jitter introduced by fine-grained random voltage fluctuations.

[TODO: add LED threshold results and discussion!]

3.5. Time-walk corrections

In order to optimize the time resolution, the time-walk caused by the height dependent timing variation based on Leading Edge Discriminator (LED) measurements has to be corrected. These time-walk corrections for the CLAS6 forward time-of-flight detector have been determined by using a laser-based calibration system [1]. This system consists of four ultraviolet (UV) lasers. The UV light is delivered to the center of each scintillator via a silica optical fiber. The TDC and ADC information from the injected laser pulses can then be used to calibrate the overall timing and pulse-height dependent time-walk.

Due to the improved time resolution of the new CLAS12 time-of-flight panel 1b the previously used method is no longer sufficient and is replaced by an in-situ calibration based on the accumulated data itself. The reasons for that are the following: a) In contrast to laser light that is delivered only to the center of the scintillator, physical data are gathered along the whole bar length. The in-situ calibration facilitates a development of position-dependent time-walk corrections, thus improving the time resolution. b) The energy distribution of the particles and the shape of the analog signals that will be used for time-walk corrections will be by definition the same as in experiment, while the laser system injects monochromatic photon pulse with preselected amplitudes not corresponding to the experimental conditions.

During development and construction and before the installation into the CLAS12 detector all scintillation counters have been evaluated and checked using cosmic ray particles. The energy deposit of cosmic muons is relatively close to that of the particles measured by CLAS12. Moreover, since cosmic muons are distributed homogenously along the scintillator, position-dependent time-walk corrections are applied. As mentioned in Sec. ?? the typically used six-bars method demands that six counters are set up one above the other and that all PMT signals are coincide.

After two days of running a sufficient amount of data was collected for each setup to carry out the analysis. The starting point of time-walk corrections procedure is ADC offsets subtraction. Fig. 18 (left plot) shows ADC distribution zoomed in offset region. The offset peak position marked by red line was subtracted from ADC values event by event. Shifted distribution is shown on the right plot of Fig. 18. For further analysis all events that correspond to the offset peak were cut away.

The next step is vertical tracks selection that is not necessary for the method itself, but needed since position-dependent procedure is going to be applied. For that purpose the TDC difference between left and right PMTs for bottom counter versus the same quantity for the top one (see Fig. 19) were plotted. These differences are divided over two since at that case they correspond to the bar length divided by effective speed of light. To determine the position of the red line

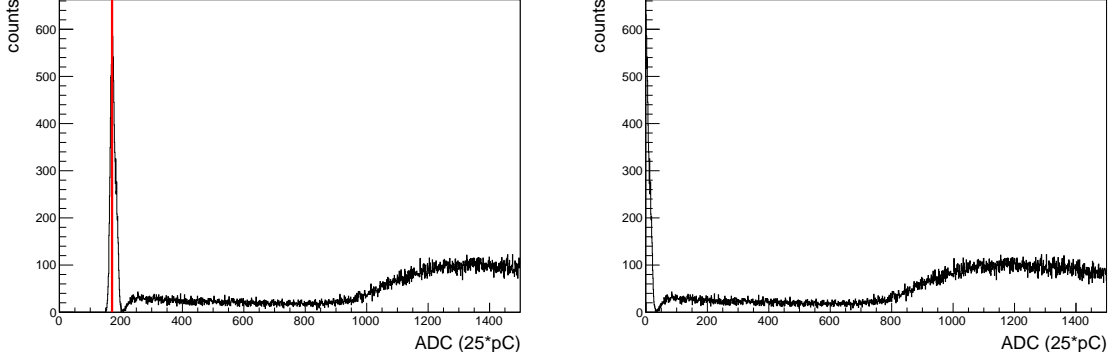


Figure 18: ADC distribution zoomed in offset region before (left plot) and after (right plot) ADC offset subtraction. Vertical red line on the left plot shows the position of the offset peak.

(see Fig. 19) one dimensional distribution of the quantity $x - y$ was plotted (see Fig. 20), where $x = (tdc1 - tdc2)/2$ and $y = (tdc11 - tdc12)/2$. These quantities correspond to the x and y axes of the two dimensional plot Fig. 19. This one dimensional distribution was fitted by gaussian to determine the mean value M (see Fig. 20). The line with equation $y = x + M$ is drawn by red on Fig. 19. For analysis the whole bar length was divided into the bins approximately 3 cm width each. The range over x-axis that correspond to the scintillator length was divided into the same number of bins. Bin size over y-axis was determined by intersections of boundaries of the bin over x-axis with red line. Events within rectangular area (shown in white on Fig. 19) were selected for further analysis. All steps described below correspond to one particular bin.

Time-walk is an instrumental pulse height dependent shift in the measured time using a leading edge discriminator [6]. This time difference is due to the finite rise time of the analog pulse reaching the threshold relative to a reference time. This effect can be minimized in hardware by using constant-fraction discriminators, or by making software corrections to the times using leading-edge discriminators. Since leading-edge discriminator is used one-parameter (λ_i) time-walk correction is applied to each PMT, where i corresponds to the PMT number. In the experimental setup reference time is given by PMT number five, which is attached to the left side of the bar number three. This PMT determines the relative timing of all the other signals. Accordingly, a single relative time depends on two parameters (λ_i and λ_{ref}) as in Eq. 3.29. In equation 3.29 the second term in each parenthesis is introduced in order to take into account signal rise time.

$$t_{corrected} = \left(TDC_i - \frac{\lambda_i}{\sqrt{ADC_i}} \right) - \left(TDC_{ref} - \frac{\lambda_{ref}}{\sqrt{ADC_{ref}}} \right) \quad (3.29)$$

For each ionizing particle path $t_{corrected}$ is ideally fixed, so the spreading σ of the Gauss fit of the $t_{corrected}$ distribution on a specified path must be minimized with the two-parameter correction

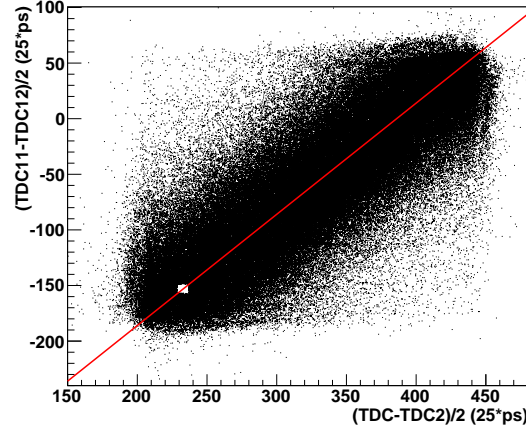


Figure 19: TDC difference between left and right PMTs for bottom counter versus the same quantity for the top one. Plot corresponds to the bars 81cm long from the set number eleven. The position of red line is determined by fitting of distribution shown on Fig. 20. Rectangular area shown in white is one of the bins that was used for time-walk parameters determination.

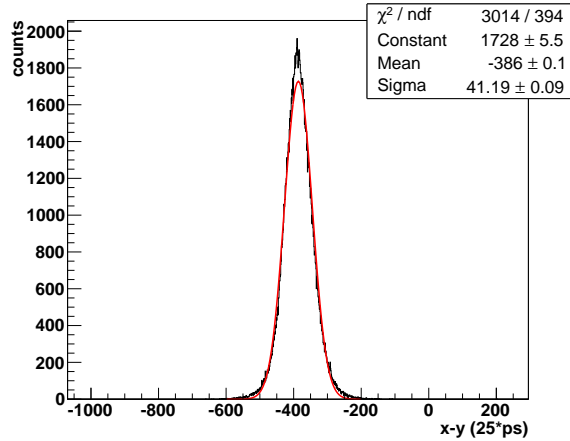


Figure 20: $x-y$ distribution, where $x = (TDC1-TDC2)/2$ and $y = (TDC11-TDC12)/2$. Mean value of gaussian fit determine position of red line on Fig. 19.

function. For that purposes each parameter λ is varied within the range from -2 to 6, where the spreading of the $t_{corrected}$ distributions is minimal, and plotted as a color code on two dimensional histograms (see Fig. 21). On Fig. 21 λ_5 versus λ_i is plotted for each PMT except PMT number six since signals from the PMTs five and six are correlated, because they are connected to the same bar. That is why to determine $\lambda_6 \lambda_7$ versus λ_6 is plotted.

In order to determine the position of the minimum each distribution from Fig. 21 is fitted by parabolic function. The intersections of red lines show positions of obtained minima. The x -coordinate of each minima gives value of λ parameters for all PMTs, except PMT five. Since almost all distributions have λ_5 as y -axis, λ_5 is determined as average value of y -coordinates of the minima for these distributions.

The procedure described above is applied for each bin from Fig. 19. On Fig. 22 all extracted λ parameters are plotted as a function of TDC differences divided by two that correspond to the length of the scintillator bar. λ -distribution for each PMT is fitted by second order polynomial. Finally for calculations of time-walk corrected times λ -parameters as smooth function of bar length is used.

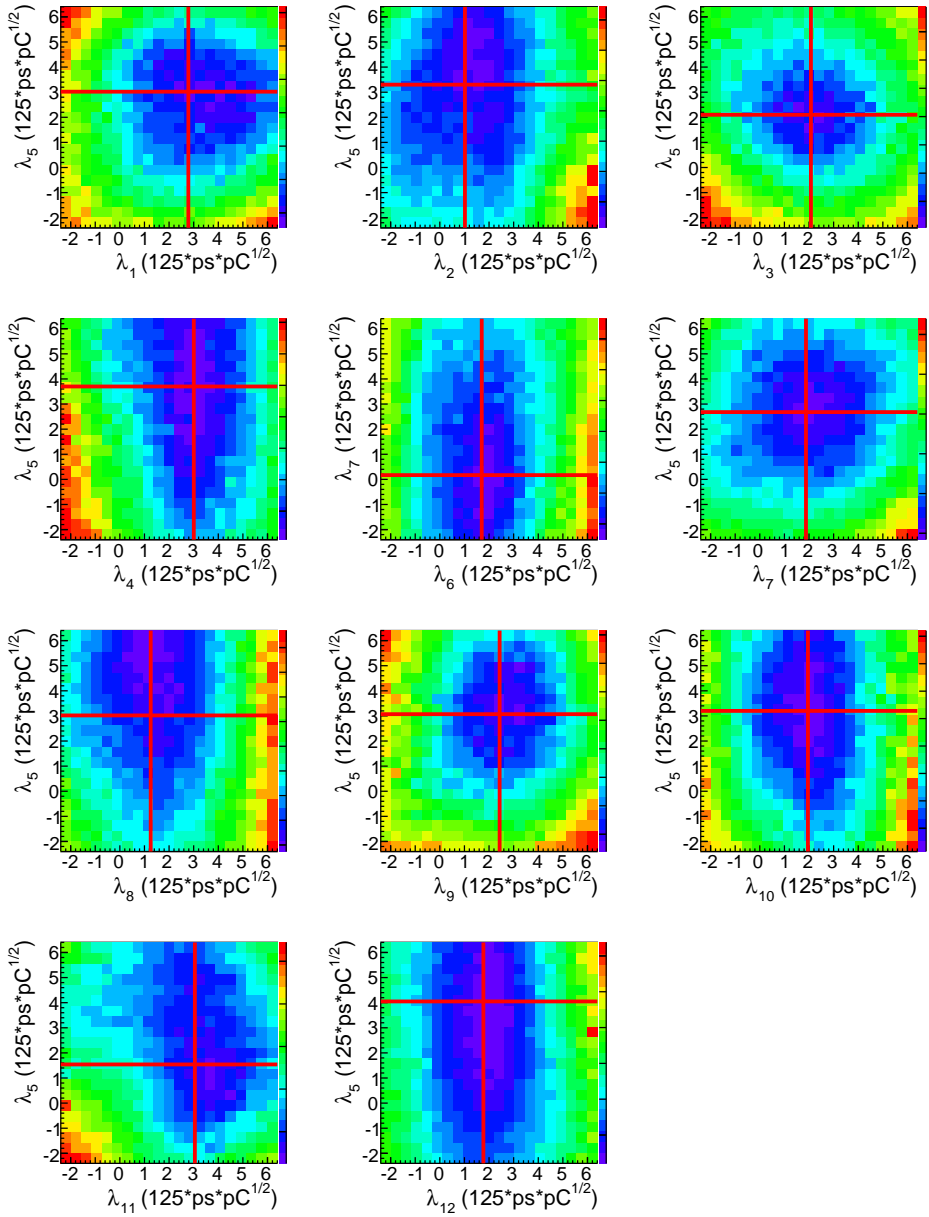


Figure 21: Two dimensional distributions used to determine time-walk parameters. Coordinate axes correspond to time-walk parameters λ_i varied from -2 to 6 each. Color code represents spreading of the $t_{corrected}$ distributions (see Eq. 3.29).

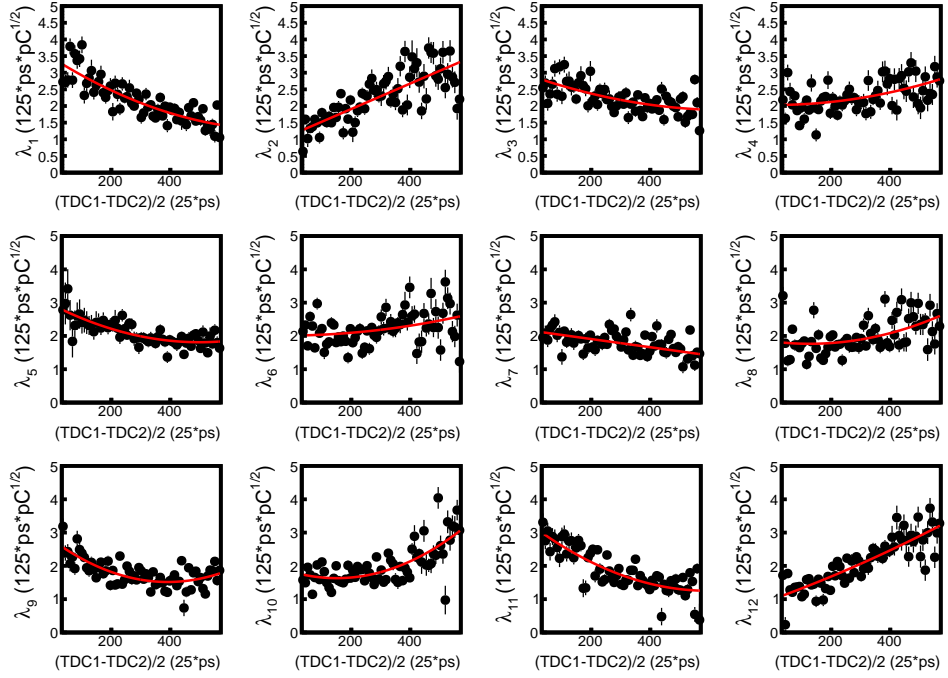


Figure 22: Time-walk parameters as function of the half of the TDC differences for the bars 200 cm long from the set number 30. Curves represent second order polynomial fit.

4. III.E. Photomultiplier tubes (PMTs)

4.1. Different PMTs time resolutions

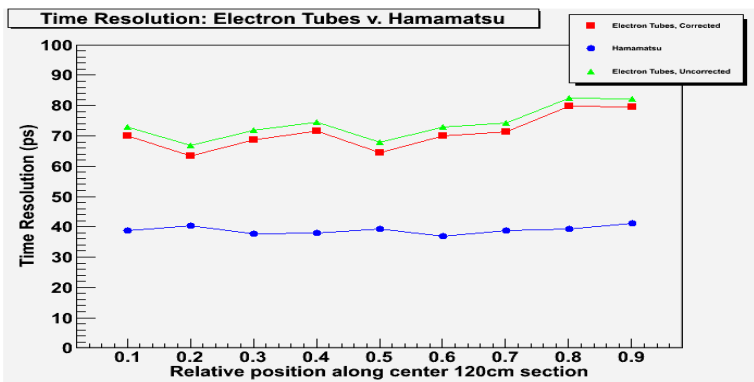
My assumptions in writing this section

1. Our chosen PMT(R9779) was compared with panel-1a PMT(EMI9954A)
2. Details of relevant differences of the tech-specs of the two PMTs and therefore the expected superiority of R9779 over EMI9954A will be listed elsewhere; here we will only give empirical proof

The selected Hamamatusu's R9779 PMTs for panel-1b were compared with Electron Tubes EMI 9954A in the 3-bar setup (*I am assuming that the 3-bar setup will either already be defined or referred to in another publication, so as to not go into details, but simply for the reader to trust that it is our way to extract time-resolution, though, it is NOT directly the time-resolution of the PMT, but of the entire counter; this is important to keep in mind, since for the old TOF system, PMT resolutions were directly compared using lasers; details of this method are in old CLAS-SC NIM paper.*)

Should I mention here that for EMI PMT tests, the contribution of the LFIO module was removed?

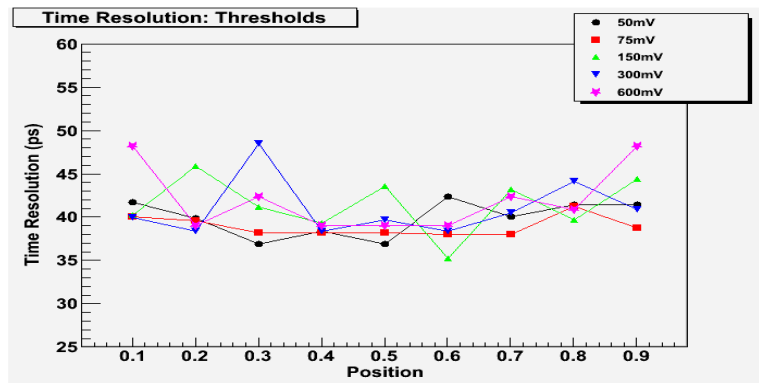
Below is the figure that shows the superiority of the R9779:



4.2. ... threshold dependence

We also compared various threshold (*Define "threshold"*) levels for the signals from the PMT and see if it had any affect on the time resolution. The threshold levels tried were: 50mV, 75mV, 150mV, 300mV, and 600mV.

Following is a figure that demonstrates varying the threshold did not affect the time resolution.



5. III.G. Magnetic shielding of the PMTs

The photomultipliers that are attached to the FTOF scintillators will be exposed to the combined stray magnetic fields from the CLAS12 solenoid and torus magnets. It is therefore important to study the effect of the magnetic field strength on the anode signal of a PMT and ultimately on the time resolution of the FTOF detector system. In the experimental test setup, a PMT was set on a flat, non-magnetic base in between a pair of Helmholtz coils and the anode signal of the PMT was digitized and processed by a DAQ system . This arrangement is shown in Fig. 1.

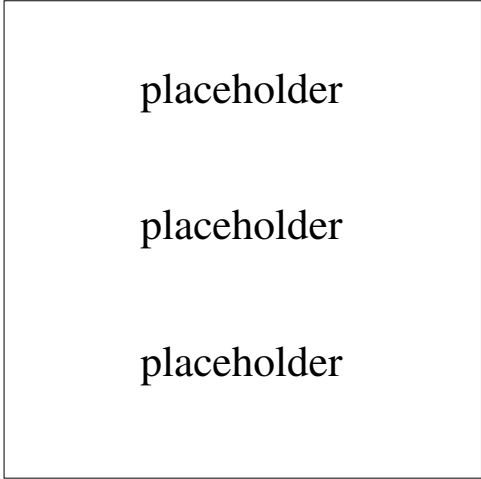


Figure 23: PMT B field test setup

Due to the dynode-array geometry of the PMT and the electrodynamic processes which finally contribute to the signal formation, the studies need to be performed in dependence of the orientation of the PMT relative to the magnetic field. Given the axial Helmholtz magnetic field, the orientation of a PMT in it can be described by two rotational degree of freedoms; their axes are illustrated in Fig. 2 and defined by the PMT's axis of cylindrical symmetry, \hat{z} and the radial axis perpendicular to \hat{z} and horizontal to the flat base supporting the PMT, $\hat{\rho}$.

In the axial Helmholtz magnetic field, a PMT can be rotated around $\hat{\rho}$ until \hat{z} is aligned transversely (T) or longitudinally (L) with the field direction. These are the two orientations in which a PMT is observed to have the two strongest and in a sense, independent responses; any other orientation is dominated by a superposition of the two responses. These two orientations are illustrated in Fig. 2.

The additional change in the signal response of a PMT when it was rotated around \hat{z} was also studied, primarily when it is already aligned in the transverse orientation (minimal to no effect due to rotations around \hat{z} is observed in the longitudinal orientation) [?] However, after implementing the final shielding configuration (see Sec. 2.2), the PMT response no longer depends on the rotational degree of freedom around \hat{z} .

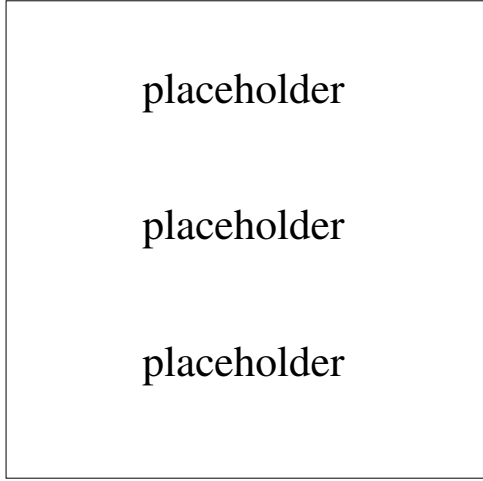


Figure 24: Tranverse and longitudinal orientations of PMT in axial B field

It is worth mentioning here that the magnetic field primarily affects the signal amplitude, while the signal shape and smoothness, which have a far larger impact on the time resolution, are mostly unaffected [?]. However, the loss of signal amplitude does affect the extracted time resolution, but only when the reduction reaches levels at which the Time-walk corrections become less efficient. Therefore, the signal reduction level was used as the parameter to quantify the response of a PMT in a magnetic field and its affect on the time resolution.

Even though it was established that when the signal amplitude is reduced by 10% in the longitudinal and the transverse orientations there is no change in the time resolution - measured to be 41 ps and 38 ps , respectively (39 ps with no magnetic field) [?] - the final design of the magnetic shielding (Sec. 2.2) is such that up to magnetic field strengths higher than those expected in CLAS12, the signal amplitude shows no reduction; the maximum stray field strength that the panel-1b PMTs are going to be exposed to is expected to be 22G at counters placed at the largest angular extent of the FTOF12 detector system, of which 2/3 (15G) will be in the axial direction [?] and the tests at USC were done with magnetic fields up to 30G, wholly directed in either the transverse or longitudinal directions.

5.1. Initial design considerations

The PMT assemblies R9779-20MOD are already manufactured with a layer of mu-metal coating. It can be seen from Tab. 1 that in the transverse orientation, compared to a PMT without any mu-metal coating, the inbuilt mu-metal shielding preserves the signal amplitude to much higher levels of magnetic fields.

| | no mu-metal | with mu-metal |
|-------|-------------|---------------|
| 10G-L | 10% | 10% |
| 10G-T | 100% | 0% |
| 15G-L | XX% | XX% |
| 15G-T | 100% | 0% |
| 15G-L | YY% | YY% |
| 15G-T | 100% | 0% |
| 20G-L | ZZ% | ZZ% |
| 20G-T | 100% | 10% |
| 25G-L | AA% | AA% |
| 25G-T | 100% | XX% |
| 30G-L | BB% | BB% |
| 30G-T | 100% | BB% |

Table 2: Reduction of PMT anode signal in various test configurations

However, even with the inbuilt mu-metal shielding, there is a rapid deterioration of the signal past 10G-L and XXG-T and this led to considering further shielding methods.

5.1.1. External shielding

In order to provide additional shielding, a rectangular external mu-metal shielding, with each side of thickness 2 mm, was designed. Tab. 2 shows that within this external shielding, in the transverse orientation, the signal amplitude is preserved up to 30 G. However, this provided no additional protection to PMT in the longitudinal orientation.

| | external mu-metal shielding |
|-------|-----------------------------|
| 10G-L | 10% |
| 10G-T | 0% |
| 15G-L | XX% |
| 15G-T | 0% |
| 15G-L | YY% |
| 15G-T | 0% |
| 20G-L | ZZ% |
| 20G-T | 0% |
| 25G-L | AA% |
| 25G-T | 0% |
| 30G-L | BB% |
| 30G-T | BB% |

Table 3: Signal reduction of PMT's anode signal in presence of external mu-metal shielding. It is observed that PMT signal's reduction is unchanged in the longitudinal orientation, but the signal is preserved to 30 G) in the transverse orientation

5.2. Final implementation of shielding with overhang

To also preserve the signal amplitude in the longitudinal orientation, it was decided that in the final implementation, the external shielding would extend a few centimeters beyond the front face of the PMT (:= overhang). This requires shaving two edges of the scintillator bars by a few millimeters. Tab. 4 shows the results of testing the signal reduction at various overhang positions of the external shielding. The overhang position of 4 cm (1.5 in) is sufficient to preserve the signal up to 30 G in the longitudinal orientation.

| | 0 cm -overhang | 1 cm -overhang | 2 cm -overhang | 3 cm -overhang | 4 cm -overhang |
|-------|-------------------------|-------------------------|-------------------------|-------------------------|-------------------------|
| 10G-L | | | | | |
| 10G-T | | | | | |
| 15G-L | | | | | |
| 15G-T | | | | | |
| 15G-L | | | | | |
| 15G-T | | | | | |
| 20G-L | | | | | |
| 20G-T | | | | | |
| 25G-L | | | | | |
| 25G-T | | | | | |
| 30G-L | | | | | |
| 30G-T | | | | | |

Table 4: Signal reduction of PMT's anode signal in presence of external mu-metal shielding at various overhang positions. It is observed that at the overhang position of 4 cm the signal is preserved up to magnetic field strength of 30 G in both the transverse and longitudinal orientations

6. Establishing an upper limit on the level of tolerable magnetic field

In the final design and implementation of the magnetic shielding, the tests show that there is going to be no reduction in signal amplitude in fields up to 30 G in the transverse and longitudinal orientation. This is already beyond the maximum fields to which the PMTs will be exposed to according to the CLAS12 design requirements [?]. However, tests were run to note signal reduction levels as the magnetic field strength was increased beyond 30 G in each of the orientations and the point at which the signal amplitude reduced by 10% in each of the orientations, transverse and longitudinal, was noted. Since up to such reduction levels, the time resolution is unaffected, the noted field strength serves as the conservative upper limit of the magnetic field at which the time resolution remains unaffected. Tab. 4 shows the results of such tests which establishes the conservative upper limit at XX G and YY G in the transverse and longitudinal orientations, respectively.

| | |
|-------|--|
| 30G-L | |
| 30G-T | |
| 35G-L | |
| 35G-T | |
| 40G-L | |
| 40G-T | |
| 45G-L | |
| 45G-T | |
| 50G-L | |
| 50G-T | |

Table 5: Signal reduction of PMT's anode signal beyond the design consideration of 30 G

6.1. Results and Conclusions

With the finally designed and implemented shielding, the time resolution of the panel-1b FTOF counters remains unaffected by the presence of fringe magnetic fields in CLAS12 up to a field level of at least $XX\;G$ and $YY\;G$ in the transverse and longitudinal orientations, respectively. This exceeds the maximum field of $22\;G$ (of which $2/3$ will be in longitudinal direction) to which the panel-1b PMTs are expected to be exposed to.

7. G Scintillator Geometry and Light guides

When a particle is passing through the scintillator, it ionizes the material and generates scintillation light. These photons travel via different paths through the scintillator, can be absorbed and reflected, then get converted by the photocathode of the Photomultiplier Tube (PMT), generating a photoelectron current. This current is amplified by the PMT and becomes a measurable electronic pulse (see Fig: (pulse) in time walk or shielding section). Finally, the pulse passes through the electronic system and is read out by the computer. All these various processes affect the total time resolution σ_{ToF} . Therefore, it is convenient to parameterize the length averaged time resolution $\overline{\sigma_{ToF}}$ by

$$\overline{\sigma_{ToF}} = \sqrt{\sigma_0^2 + \frac{\sigma_1^2 + (\sigma_p \frac{L}{2})^2}{N_{pe} \exp(-\frac{L}{2\lambda})}}. \quad (7.1)$$

The parameters in this equation quantify the characteristics of the detector geometry and components, here, σ_0 is the intrinsic resolution of the electronics and other processes that are independent of the light intensity, σ_1 models the jitter in the combined single-photoelectron response of the scintillator and PMT, and σ_p accounts for path length variations in the light collection. The distance from the source to the PMT, which for $\overline{\sigma_{ToF}}$ is taken to be half the length of the counter($\frac{L}{2}$), and λ is the attenuation length of the scintillator. N_{pe} is the average number of the photoelectrons seen by the PMT of a counter with an infinitely long attenuation length. The statistical behavior of σ_1 and σ_p is encoded by scaling the single-photoelectron responses by $\sqrt{N_{pe}}$.

The geometry of the individual FToF12 detectors has to be optimized, since it influences the time resolution. Figure 25 uses equation 7.1 to show how the length, width, and thickness of detectors typical for the CLAS12 design requirement affect the time resolution, where the parameters of the time resolution for the existing panel 1a counters are given in Ref [?]. The design requirement for panel 1b is to achieve a combined time resolution for panel 1a and 1b of 80 ps for all scintillators up to 4 cm length.

The most obvious improvement of the time resolution of a detector can be accommodated by increasing the photon statistics N_{pe} , since the time resolution is proportional to $\sqrt{N_{pe}}$. The number of photons reaching the photocathode scales with the ratio of PMT entrance over exit window areas and the thickness of the scintillator. Given the same PMT diameters, changing the geometry (width \times thickness) from $15 \times 5 \text{ cm}^2$ to $6 \times 6 \text{ cm}^2$ leads to an increase of N_{pe} by $\frac{15}{6}$. The loss of light from a scintillator can occur in two basic ways; one is the escape of light at the scintillator surface. The simplest and most common practice is to redirect escaping light by total reflection. To maximize the internal reflection, any reflecting film should be loosely wrapped with an air gap to the scintillator, which is described in Sec.I. The other one is through absorption by the scintillation material itself, which is related to the attenuation length consideration described in

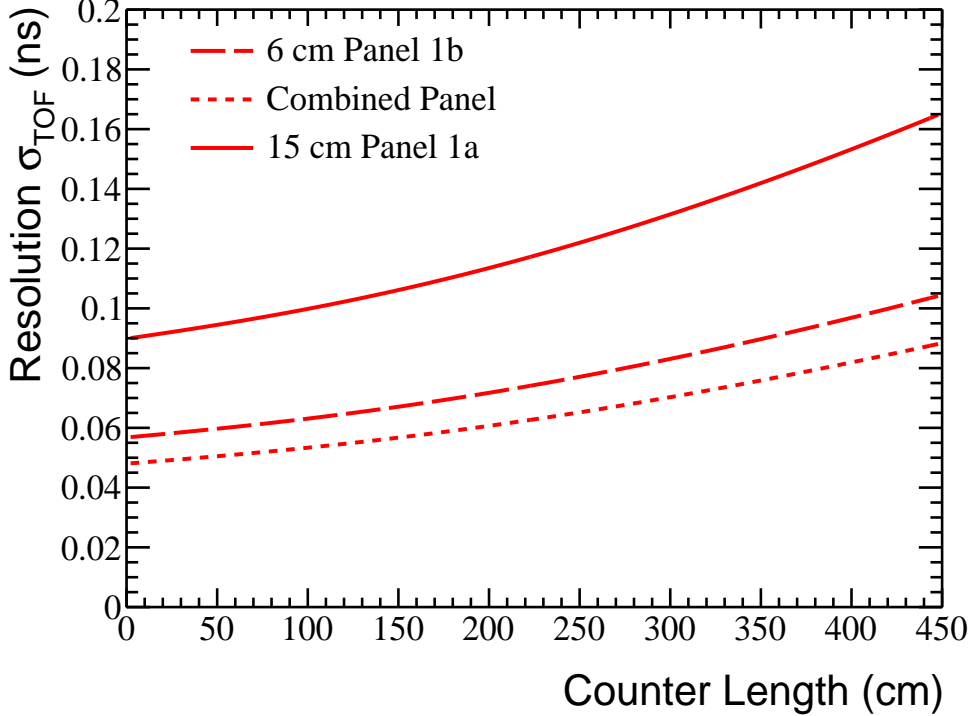


Figure 25: Solid line, the measured and parameterized average standard deviation $\overline{\sigma_{TOF}}$ time resolution of the existing panel-1a counters (15 cm wide, 5 cm thick) fit with an assumed intrinsic electronic resolution of 40 ps [?]. Scaling the parametrization by $\sqrt{\frac{2}{5}}$ leads to the Long dashed line representing the new panel-1b counters (6cm wide, 6cm thick) and short dashed line the combined panel-1a and panel-1b counters time resolution.

Set.H.

In contrast to the total reflection requirement discussed above, for the coupling between the scintillator and the PMT, the refraction index change should be minimized to maximize light transmission. Additionally, the PMT is often coupled to the scintillator by a light guide to match the geometry of scintillator to the circular entrance surface of PMT, as in the case of the FTof panel 1a detectors. In the prototyping phase, simulations done to optimized the shape and length of light guides coupling the square exit window of the scintillator to the circular PMT entrance window were carried out. Under best conditions a monotonically increasing amount of light is lost up to a light guide length of 6 cm, which would already limit the over all acceptance of the CLAS12 detectors. Hence the simulation shows that the best light transmission is achieved when the PMT is directly attached to the scintillator. The result was experimentally verified by comparing the scintillator without and with 7cm-long light guide. In order to quantify the time resolution with or without light guide, three-bar time resolution measurements described in Sec. III B were utilized to extract the time resolution of the middle bar under both conditions, respectively. Without light guides, the Hamamatsu PMTs were directly mounted to the left and right ends of a $5 \times 5 \times 150$ cm³ BC408 scintillator. With light guides, the light guides were first wrapped with aluminized mylar

and then attached to both ends of the same $5 \times 5 \times 150 \text{ cm}^3$ BC408 scintillator, and the same Hamamatsu PMTs were mounted to light guides. Figure 26 shows that the average time resolutions

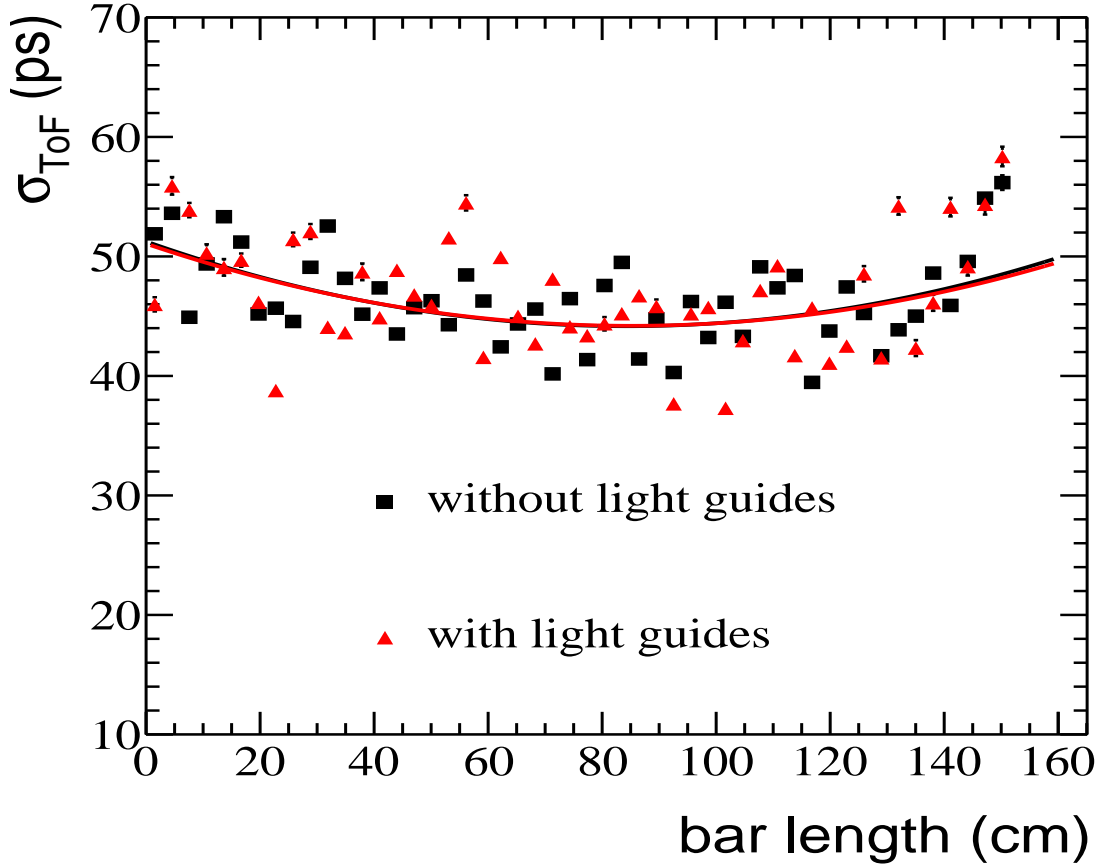


Figure 26: Black squares, position dependent time resolution of a $5 \times 5 \times 150 \text{ cm}^3$ BC408 scintillator with and red triangles without light guides.

of scintillator with and without light guides are 46.879 ps and 46.519 ps , respectively. Even though, the time resolution of scintillator without light guide is a slightly better, the influence of the light guide is still negligible with in error bars, eliminating the light guides allows for long scintillators covering full fiducial region of CLAS12.

8. H Scintillator

Since the time resolution is proportional to $\sqrt{N_{pe}}$, in order to improve the time resolution, the scintillator material for the TOF system must have fast decay times, long attenuation length, and good spectral match to the PMTs. The attenuation length of scintillator can be divided into two parts. One part is called the technical attenuation length (TAL), which is defined as the length reducing the amount light by a factor e and which depends on the geometry the scintillator and the reflective properties of its surface. The other part is called bulk attenuation length (BAL), which reduces the initial light intensity by a factor e according to the Buger-Lambert Law and which depends on the transparency and the scintillation material. From the design requirement, the counter length of CLAS12 panel 1b detectors varies from 17.27cm to 407.9cm , so it is important to find the right material for all counters. The Table 6 shows that scintillator material *EJ200* and *BC408* both have longer attenuation length and slower decay time. *EJ204* and *BC404* both have shorter attenuation length and faster decay time. The time resolution of these scintillator material for 50 cm -long bars are measured. The comparison results are shown in Fig. 27, there is no big difference between different material.

| Plastic Scintillator | Decay Time |
|----------------------|--------------|
| EJ200 | 2.1ns (slow) |
| EJ204 | 1.8ns (fast) |
| BC408 | 2.1ns (slow) |
| BC404 | 1.8ns (fast) |

Table 6: Scintillator comparing

The parametrization of $\overline{\sigma_{ToF}}$ is used to study the possible improvements in time resolution based on a trade-off between the decay time of the scintillator and the number of photoelectrons arriving at the PMT, which depends on the attenuation length [?]. Fig. 31 shows the expected time resolution plotted as a function. Based on the fast decay time of *BC404*, it is used as shorter bar's material. For longer counters, the existing material *BC408* with its larger attenuation length is the better choice. In the Fig. 31 there is a time resolution crossing point around 200 cm . Below it, the counters with *BC404* material have better time resolution and above it, the *BC408* counters have better time resolution. From the above information, we decided to use *BC404* material for the length of counters shorter than 200 cm and *BC408* material for the counters longer than 200 cm .

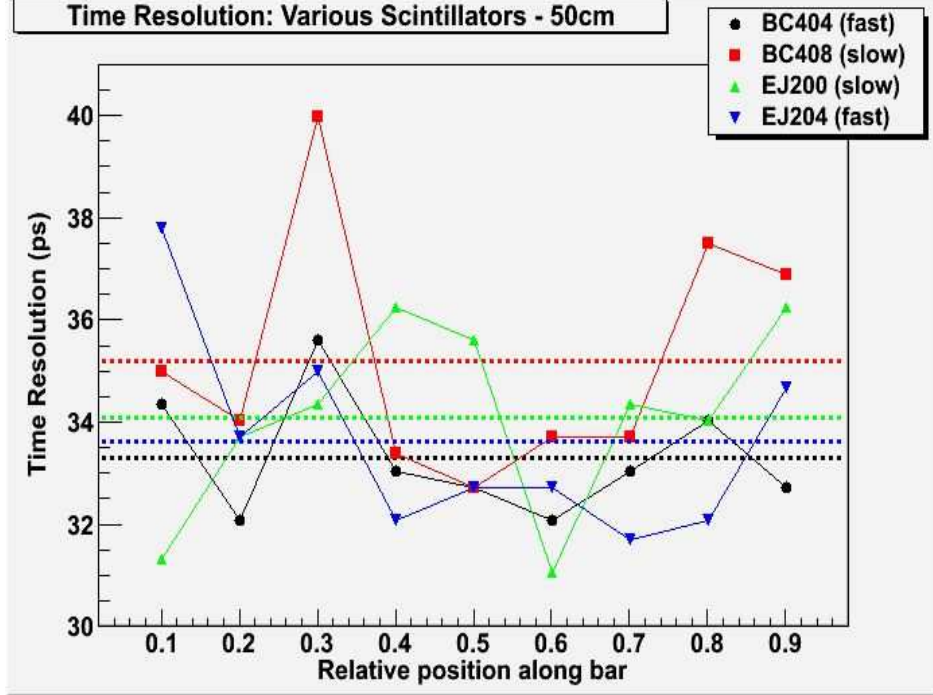


Figure 27: The time resolution of different scintillator material (50cm scintillator bars)

Initial measurements show that attenuation length values vary even among scintillation bars of the same material and from the same mold, so in order to verify that each counter meets required specifications, the attenuation length measurement is incorporated into the unit testing of each counter constructed for Panel 1B. There are two methods used to measure the attenuation length. One is the cosmic ray method, which we use the same data collected in the three-bar time resolution measurements, described in Sec.III B. Figure 29 shows the Offset-corrected ADC values, which are directly proportional to the number of photons arriving at the photocathode are plotted against TDC difference values ($\frac{TDC_L - TDC_R}{2}$) (also called Δt), which are proportional to the position through which the ionizing particles pass. To find the maximally occurring ADC value for each Δt slice, ADC distributions for each TDC difference interval are fit with Gauss-convoluted Landau functions. The ADC provides a measure of the number of photons reaching the photocathode, and the left and right TDCs provide the time information needed to reconstruct the impact position based on the effective speed of light in the scintillator. The attenuation length parameters, TAL and BAL, of the scintillator are given by,

$$N = N_{0T} e^{-\frac{x}{\lambda_T}} + N_{0B} e^{-\frac{x}{\lambda_B}} \quad (8.1)$$

where $N_0 = N_{0T} + N_{0B}$ is the initial number of photons caused by the cosmic ray passing through the scintillator at the impact position x and N is the number of photons arriving at the PMT. Figure 28 illustrates the relationship between N (ADC) and $x((TDC_L - TDC_R)/2)$ for the data.

Slices of the TDC difference values are projected onto the ADC axis, and fit with Gauss-convoluted Landau functions from which the most probable ADC value for each position is obtained (Fig. 29). These new pairs of data points are fit by various ansätze of exponential functions to extract the attenuation length parameters, as shown in Fig. 30.

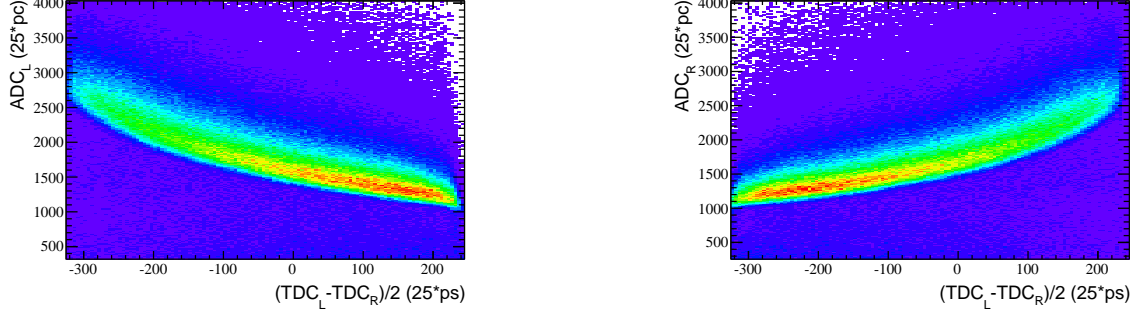


Figure 28: Left and right ADC_L and ADC_R versus TDC difference for a $6cm \times 6cm \times 210cm$ bar

And the other is the source method, the $Sr - 90$ source was put on the top of one scintillator at $5cm$ away from left side, then use the same electronic setups as three bar method. After the data satisfy the statistic requirement, move the source to the position of $15cm$ away from left side of the bar and repeat the same step. For the position part, there is $10cm$ away between each measurement position point. After the measurement, the data analysis steps are similar with the cosmic ray method, the only different is the ADC value which is subtracted by the cosmic ray signal background. After subtracting, fit the mean value of the ADC distribution of the fixed position versus the position distribution by the exponential function 8.1 to get the TAL and BAL attenuation length, which shows in Fig.6. Here, it is a improvement that the attenuation length have two components, can not be fit well by the single exponential function.

Finally, in order to compare with the factory attenuation length value, we use two points method to get the attenuation length (same method as factory used to get their attenuation length value using laser system?). The two positions($15cm$ and $195cm$ away form the left side of the bar) are chosen to get the ADC values, and then fit this two data points by one exponential function to get the corresponding attenuation length. The comparison results are shown on Table 7 and Table 8. we got consistent attenuation length value less than the factory value with both cosmic ray and source measurements, but for the first order acceptable. This is one of the quality check procedure.

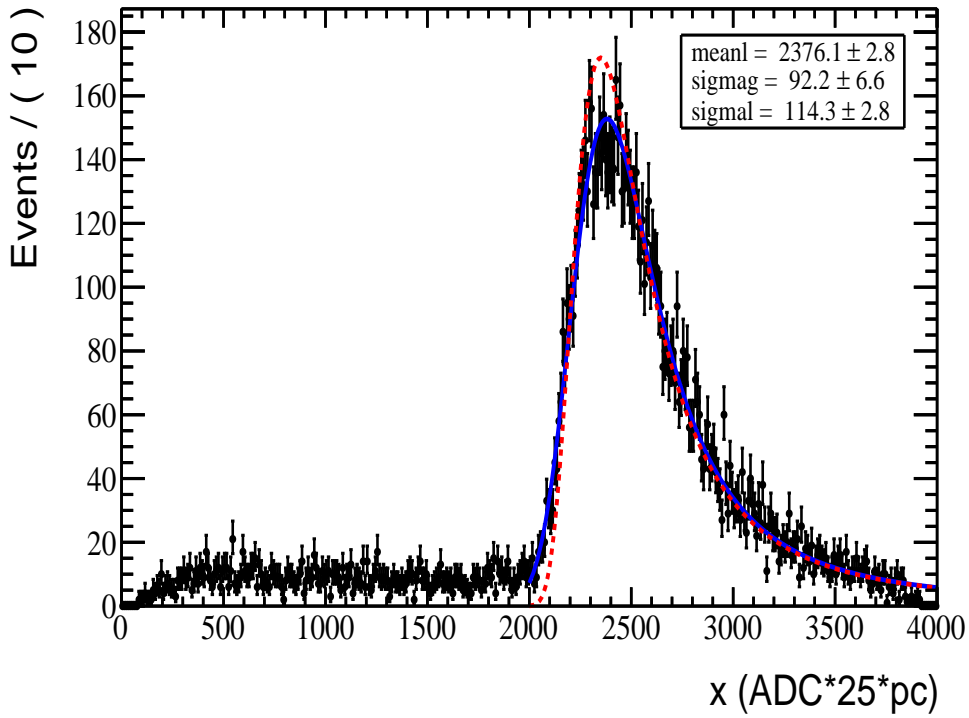


Figure 29: Gauss-convoluted Landau fit of the ADC distribution for a central single TDC difference slice for the BC-408 210 cm-long bar, where x represents the ADC value, and "Maximum x" is hence the most probable ADC value. The blue line shows Gauss-convoluted Landau fit, the red dashed line shows Landau fit only.

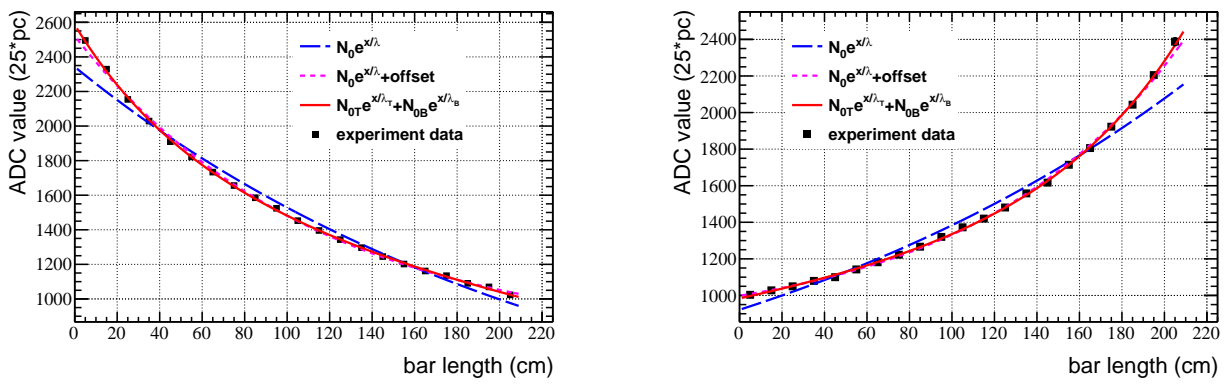


Figure 30: ADC versus TDC difference for the left and right PMTs of the BC408 210cm-long bar. The black square shows most probable ADC value points corresponding to the bar length , the red line shows two exponential function fit, the blue long dashed line shows on exponential fit, the magenta short dashed line shows one exponential function with offset fit.

| Scintillator type | PMT Position | 2 points AL (cm) | | 2 points AL (cm) | | 21 points AL (cm) | |
|---------------------------|--------------|------------------|-----------------|------------------|-----------------|-------------------|--------------|
| | | (15 and 195 cm) | (25 and 185 cm) | (35 and 175 cm) | (45 and 165 cm) | BAL | TAL |
| LAL Factory AL (280cm) | Left | 178.09 ± 0.27 | 181.96 ± 0.34 | 185.98 ± 0.39 | 188.24 ± 0.46 | 250.03 ± 1.37 | 43.34 ± 0.47 |
| | Right | 238.06 ± 0.50 | 252.89 ± 0.63 | 261.51 ± 0.77 | 276.94 ± 1.00 | 332.33 ± 0.89 | 26.59 ± 0.20 |

Table 7: Attenuation Length (AL) Table (210 cm bar) Source Method

| Scintillator type | PMT Position | 2 points AL (cm) | | 2 points AL (cm) | | 21 points AL (cm) | |
|---------------------------|--------------|------------------|-----------------|------------------|-----------------|-------------------|-------------|
| | | (15 and 195 cm) | (25 and 185 cm) | (35 and 175 cm) | (45 and 165 cm) | BAL | TAL |
| LAL Factory AL (280cm) | Left | 231.31 ± 8.09 | 234.95 ± 7.78 | 240.84 ± 9.51 | 241.45 ± 11.89 | 330.6 ± 43.1 | 48.3 ± 12.7 |
| | Right | 235.85 ± 8.61 | 240.33 ± 10.82 | 242.51 ± 11.00 | 241.97 ± 11.73 | 462.0 ± 167.1 | 58.8 ± 18.1 |

Table 8: Cosmic Ray Method

*AL—Attenuation Length *LAL—Long Attenuation Length *2 points—1 exponential function method *BAL—Bulk Attenuation Length

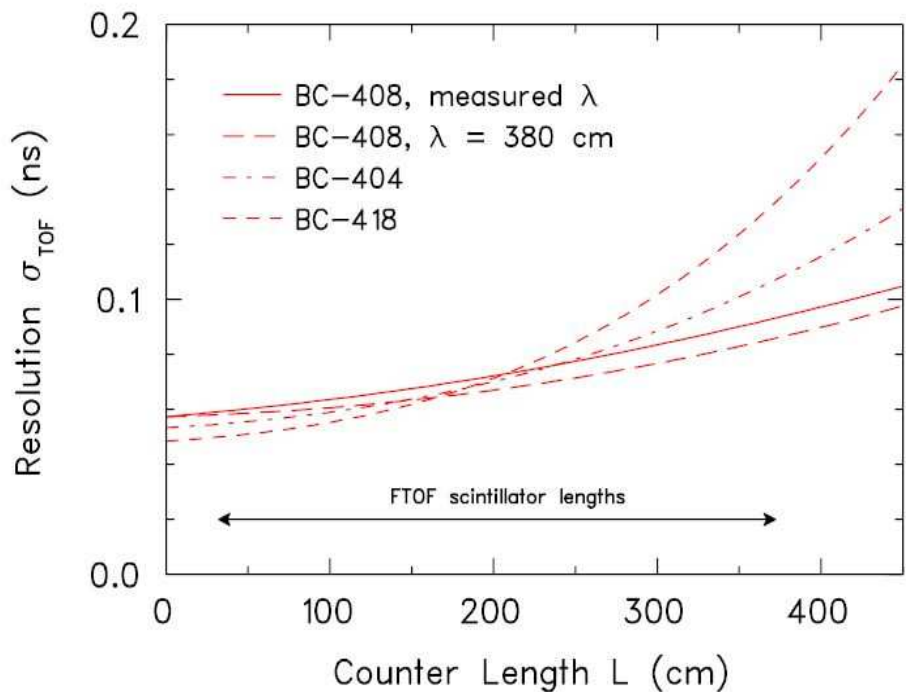


Figure 31: Resolution for various scintillation materials showing the trade-off between attenuation length and decay time [?]

9. I Reflective wrap

In order to maximize the internal reflection to get better time resolution, choosing the right wrapping material became important, so the following study was done for this purpose. One BC404 $6 \times 6 \times 120\text{cm}^3$ scintillator is wrapped using one layer of aluminized Mylar and several layers of Tedlar. Another same size scintillator is wrapped using one layer of the white paper material and the same amount of Tedlar. Hamamatsu PMTs serial FA0413 and FA0389 are mounted to the left and right ends, respectively, of the scintillator with the VM2000 wrapping and aluminized Mylar wrapping material. The detector is then placed as the middle bar in the 3 bar setup and voltages are set so as to bring the point of inflection on the ADC histograms to around 1000. Thresholds are set to 75mV. Data is collected until 180000-200000 events are recorded.

By comparing the time resolution of a scintillator bar wrapped in the VM2000 material with it in aluminized Mylar material, Fig. 32 shows that the VM2000 material does not yield significantly better time resolutions than the aluminized Mylar material. It was also noted that the setup with the white paper wrapping required greater voltage to achieve points of inflection around 1000 on the ADC histograms. Finally, we decide to use the cheaper aluminized Mylar as the wrapping material.

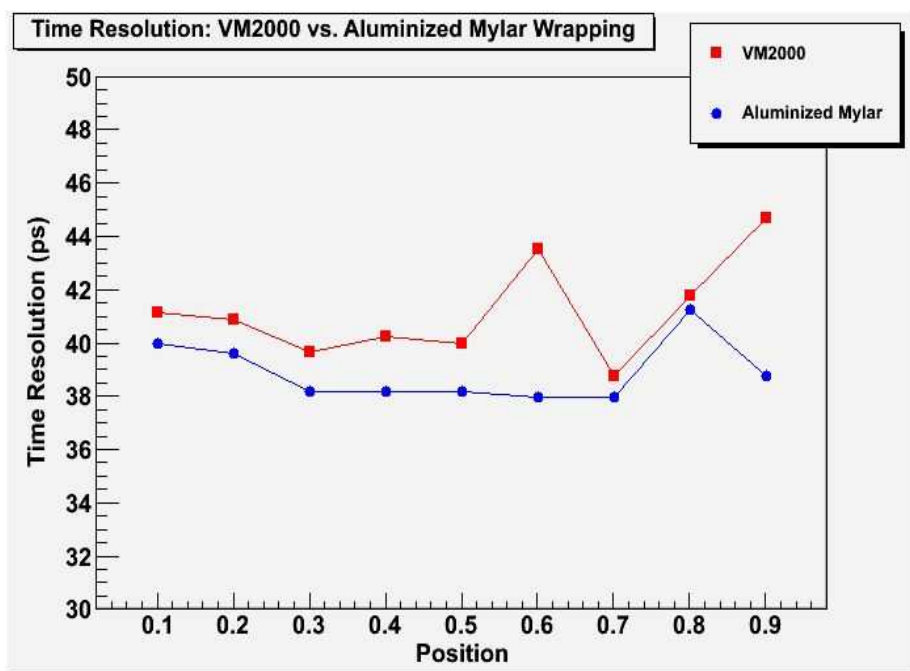


Figure 32: Wrap material

10. J Cables

The primary concerns regarding choice of cable type are cost, space, and impact on time resolution. Low-attenuation cables that maintain signal integrity over long distances cost more and occupy more space. And the fast timing of signals from the FTOF system requires cables with low signal distortion also. With the cables of 768 PMTs [7] being routed between the layers and panels of the detector, the extra volume of bundled cables is a serious concern, so barring an impact on time resolution, the thinner and less expensive RG58 cables are preferred. The distortion and attenuation of signals through five different types of cable was investigated, including specification measurements of signal speed, attenuation, and rise time, which were all listed in the Table 9. After choosing the RG58 cable, the rise time and amplitude of the signal with RG58 cable length varied from 100 *ft* to 500 *ft* were measured, and the results are shown in Table 10.

Additionally, and most importantly, the time resolution tests were performed for various lengths of cable RG58. The results are shown in Table 11, the time resolution does not change to bad even for 100 feet-long cable. And with the digitization electronics at the panel edges, the maximum cable lengths would be under 21 ft, for which RG58 is still well-suited.

| Cable Type | Cable Length | Delay Time | Signal Speed | Amplitude | Rise Time (30% to 70%) | Rise Time (10% to 90%) |
|------------|--------------|------------|--------------|-----------|---------------------------|---------------------------|
| RG-9913 | 251.5 ft. | 303.7 ns | 25.24 cm/ns | 1.4 V | 1.78 ns | 10.55 ns |
| RG-8 | 202.2 ft. | 310.6 ns | 19.84 cm/ns | 1.432 V | 2.69 ns | 12.69 ns |
| RG-174 | 128.2 ft. | 198.35 ns | 19.7 cm/ns | 1.072 V | 4.30 ns | 18.03 ns |
| RG-214 | 95.3 ft. | 147.4 ns | 19.71 cm/ns | 1.464 V | 1.36 ns | 7.01 ns |
| RG-58 | 200 ft. | 323.3 ns | 18.86 cm/ns | 1.41 V | 5.67 ns | 22.04 ns |

Table 9: Individual cable comparison table (gate width:80ns)

| Cable Length | Amplitude | Rise Time (30% to 70%) | Rise Time (10% to 90%) |
|--------------|-----------|---------------------------|---------------------------|
| 5 ns | 1.55 V | 0.36 ns | 1.05 ns |
| 50 ft. | 1.54 V | 1.03 ns | 5.37 ns |
| 75 ft. | 1.50 V | 1.9 ns | 10.94 ns |
| 100 ft. | 1.47 V | 2.80 ns | 15.39 ns |
| 200 ft. | 1.42 V | 7.20 ns | 37.77 ns |
| 300 ft. | 1.36 V | 12.88 ns | 56.87 ns |
| 400 ft. | 1.28 V | 18.34 ns | 76.22 ns |
| 500 ft. | 1.24 V | 24.65 ns | 93.38 ns |

Table 10: Variable length comparison results of RG58 cable (gate width:80ns)

| Cable Length | Time Resolution |
|--------------|-----------------|
| 50 ft. | 36.16ps |
| 75 ft. | 36.53ps |
| 100 ft. | 34.37ps |

Table 11: Time resolution results of 100cm reference bars with different RG – 58 cable length

11. F Counter construction and testing process

The CLAS12 panel 1b detector has 62 counters. Each counter contain one scintillation bar wrapped with aluminized Mylar film and two PMTs covered with magnetic shielding boxes. For counter assembly, each end of the scintillator is fitted with black tape (hereon referred to as "anticookie"), which masks the corners while leaving a circular window that extends one millimeter into the area that will be covered by the PMT. Apply approximately 1 *ml* of glue to the top end of a scintillator, straight down in the center of the anticookie. Check for bubbles in glue. Since the bubbles between scintillation bars and PMTs can influence the time resolution, reapply glue to avoid bubbles. Lower the PMT in a rotating motion through the centering tools slowly onto the scintillators.

After gluing two PMTs on the end of one scintillator, the Tedlar film was wrapped the counter tightly and wrinkle-free in three layers. Retain the film tension with electrical tape, secured only on the front side. Finish it off with a layer of the 5-cm wide, thin, black tape running the full length of the Tedlar sheet to avoid peeling off. Wrap 2 layers of electrical tape around PMT about 3 cm from edge of scintillator and at end near wires. Firmly pigtail the Tedlar film as close as reasonably possible to the PMT high voltage (HV) divider in the center with the electrical tape, trim the Tedlar to 3 cm from the PMT HV divider, and finish the pigtail by wrapping the electrical tape around the bundled Tedlar and cables extending to 5 cm beyond the PMT HV divider. Check that the ends closest to the PMT of the Tedlar pigtail are less than 15.5mm in diameter in order to pass through the cable hole of the magnetic shielding box. Zip tie wires tightly using pliers at base of PMT and trim excess.

Repeat above steps for the same length six bars, then ensure that the six counters are properly aligned and secured in the six-bar rack. Connect HV, anode, and dynode cables, each set from top-left, labeled 1 to bottom-right, labeled 12. Apply baseline voltages according to PMT testing task database entries. Verify that the anode and dynode signals on the oscilloscope match the nominal documented pulse-shape distribution. Verify that the dark current is independent of light on/off status. And then start to take test run. After enough statistic data taken, the automated analysis program (section IV part G) will get the attenuation length and the time resolution of the individual counter and saved them in the database.

The backing structure is designed to support the counters in the detector space, each backing structure holds two neighbor length counters , which shows in Fig. 33. There is a single-sided rubber tape between the backing structure and counters, which is in order to prevent counters to move around. Lefthanded and righthanded double-sided fiberglass tape loops, running side-by-side extending from the back corner along the back, the side, and then across the top surfaces in

opposite directions, which shows in Fig. 34, binds two counters and the backing structure tightly together. Figure 36 shows the example of double-sided fiberglass tape distribute in one backing structure precisely. Since two scintillators have different length, the close end position can only tolerate one single direction tape loop. Then applying a single-sided, red Mylar tape loop, with both ends terminating on the back of the backing structure, to cover the double-sided fiberglass tape to avoid the peeling, which shows in Fig. 35. After considering the room tolerance between scintillators, it is important to make sure there is no overlapping tape loop between all backing structure. The nice whole tape loop distribution for all counters is shown in Fig. 37. Repeat above taping steps for all backing structure and assemble them as six sectors, one of them shows in Fig. 37.



Figure 33: Counter structure

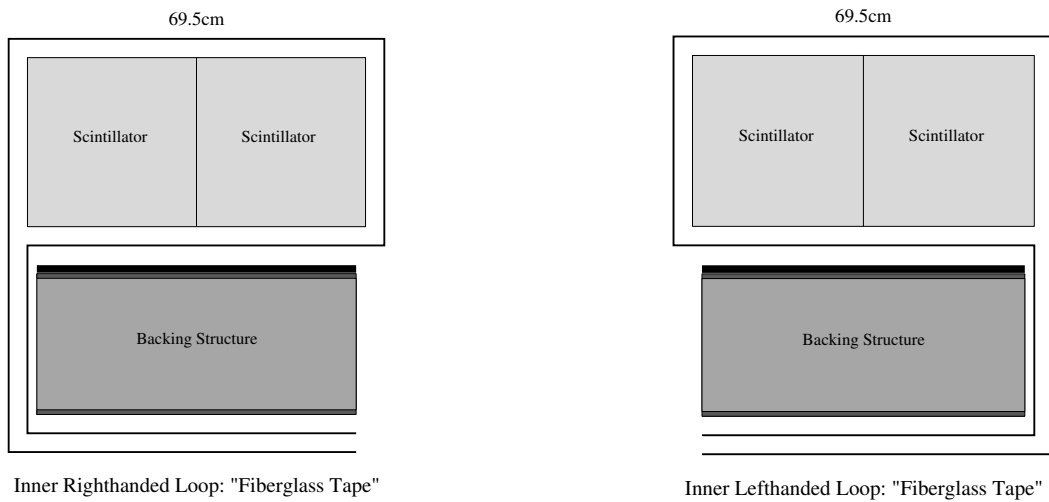
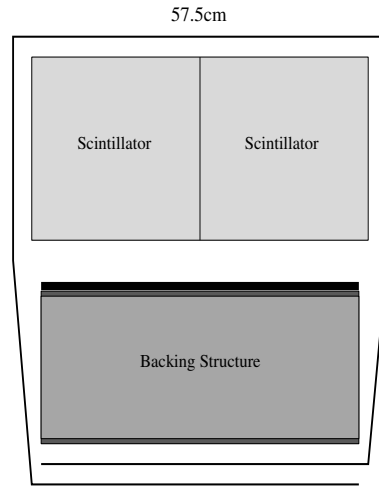


Figure 34: Taping direction



Outer Wrap Loop: "Red Mylar Tape"

Figure 35: Counter structure

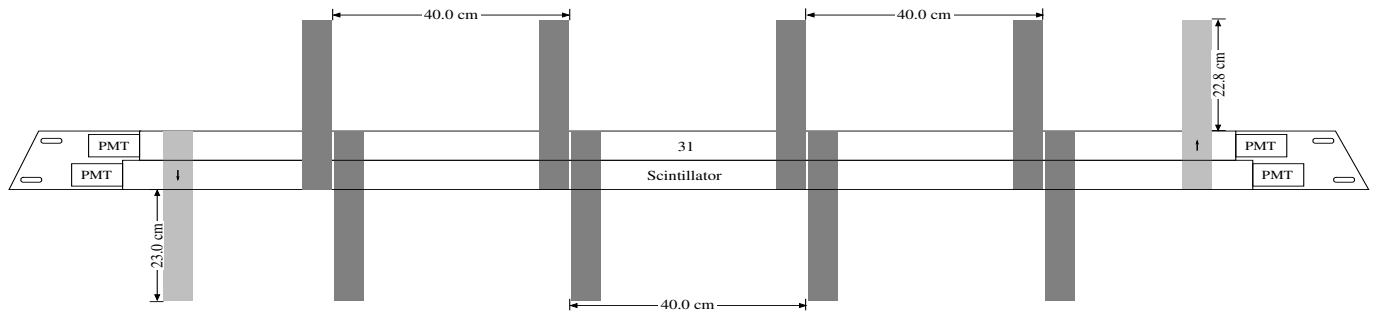


Figure 36: wrapping example of sector 31

The following section is relate to the technical detail about PMT testing, counter assembly and testing. It can be escaped.

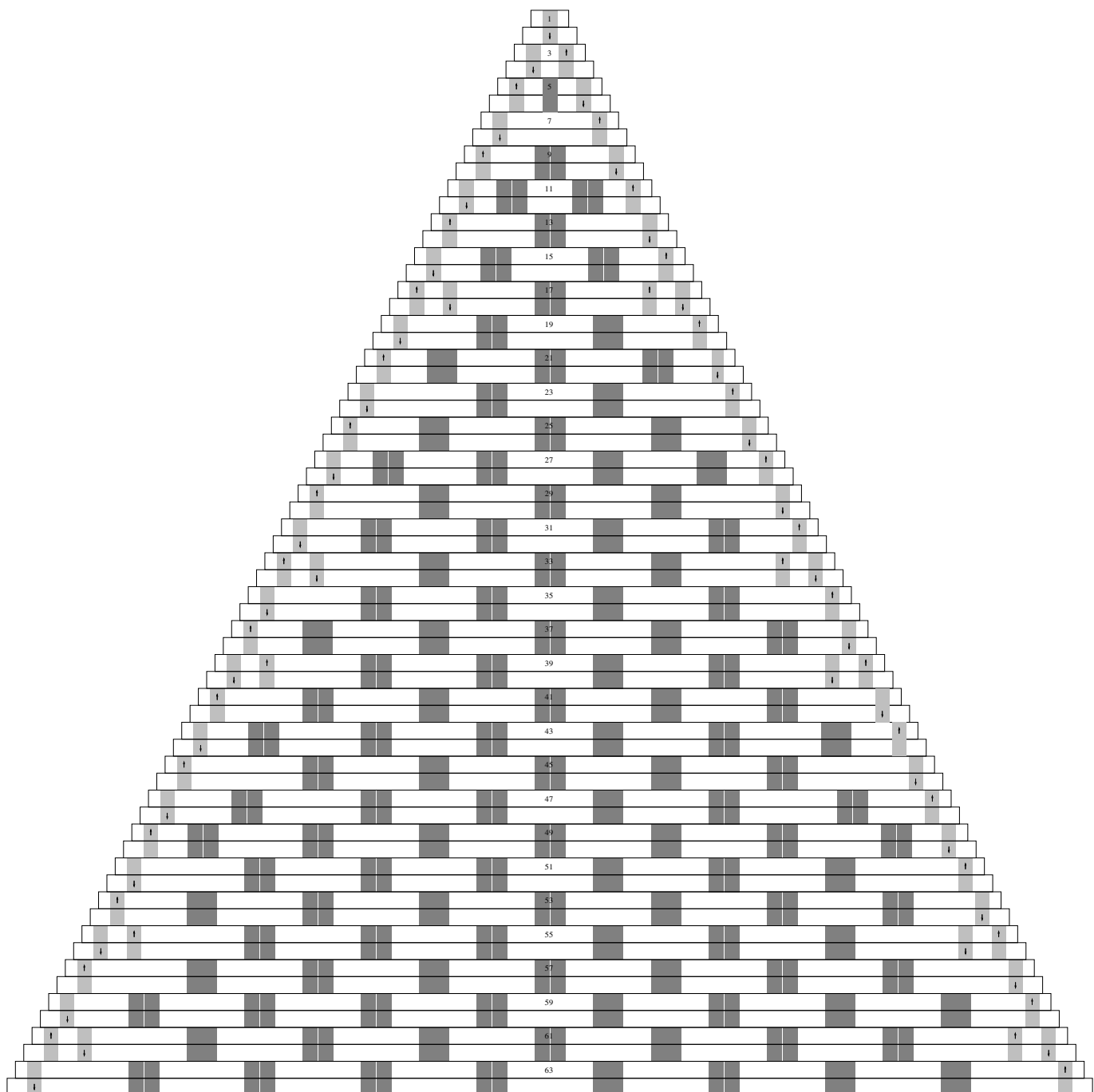


Figure 37: Final taping structure of all sectors

12. PMT testing, counter assembly and testing technical detail

PMT Testing

For quality assurance of the photomultiplier tubes and counter assemblies used in the CLAS12 1b detector panel, a set of testing procedures was developed. During the testing procedures some precautions were made in order to preserve the internal electronics of the PMTs. In order to prevent overcurrent in the PMTs the high voltage was to never exceed 1750 V and the PMT was never exposed to light while the high voltage was on.

The testing procedures began with unpacking the PMTs, connecting the high voltage cable to the power supply and the anode and dynode cables to (**). The PMT with attached cables was then loaded into the light tight testing box. *Should there be a diagram?* In doing this the PMT was placed flush against the scintillator and affixed with optical grease in order to decrease light leakage.

A set of [baseline measurements](#) is conducted in order to • **Baseline measurements**

- Remove the source.
- Feed the anode signal into the Linear FiFo; one output going to the discriminator with a threshold of 10mV and output directly to a visual scalar. The second output should go to the oscilloscope.
- For scalar measurements, remove the VETO for 100 seconds and record the count on the scalar
- For Oscilloscope measurements, set vertical scale to 20mV, adjust trigger to 10mV, and take a range of frequency values and average
- [Would like to see what these measurements are.](#)
- 1500V ADC
- Record (ADC mean - offset mean).
- Perform 2 times.
- For ADC measurements use the voltage splitter at 1500V even if not needed
- Baseline ADC
- [Is this supposed to be repeated?](#)
- adjust HV to baseline
- Record (ADC mean - offset mean).
- Perform 2 times.
- For ADC measurements use the voltage splitter even if not needed
- Baseline rate of events
- [Is this supposed to be repeated?](#)
- Feed the anode signal with source into Linear FiFo; one output going to the discriminator with

a threshold of $10mV$ and output directly to a visual scalar. The second output should go to the oscilloscope.

- For scalar measurements, remove the VETO for 100 seconds and record the count on the scalar
- For Oscilloscope measurements, set vertical scale to $20mV$, adjust trigger to $10mV$, and take a range of frequency values and average

• **Baseline dark current: How should these plots look?**

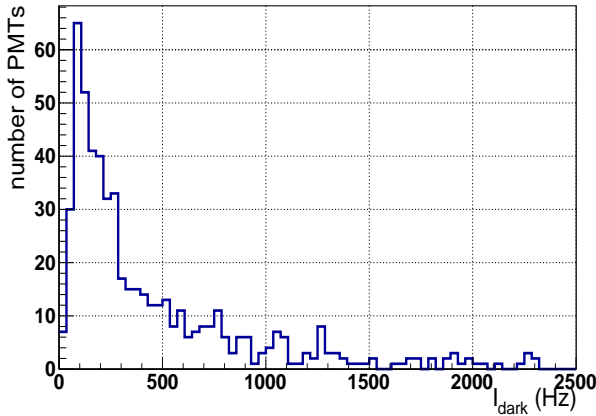


Figure 38: Measured dark current

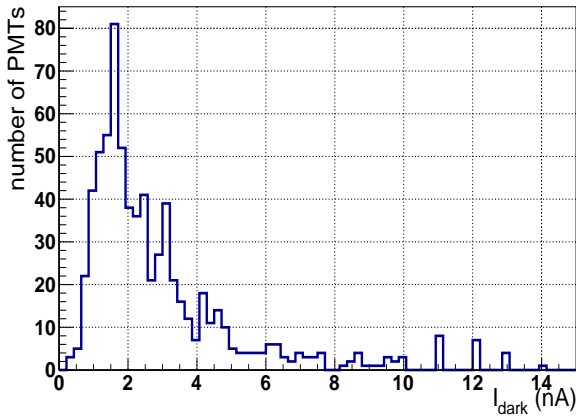


Figure 39: Factory dark current

- Is this supposed to be repeated?
- What is different about each repeated measurement? What is each set of measurements for?
- Could this be stated once and then referred back to?
- Feed the anode signal into the Linear FiFo; one output going to the discriminator with a threshold

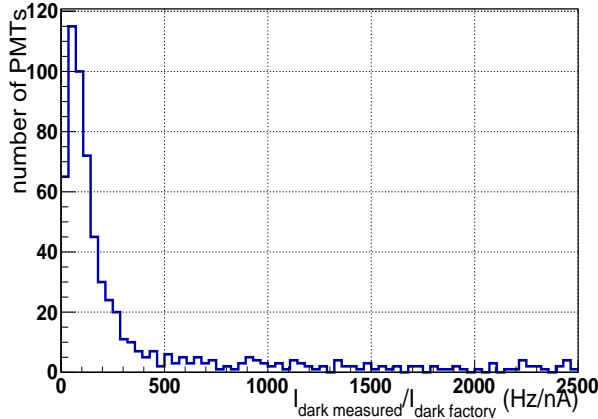


Figure 40: Factory and measured dark current ratio

of $10mV$ and output directly to a visual scalar. The second output should go to the oscilloscope.

- For scalar measurements, remove the VETO for 100 seconds and record the count on the scalar
- For Oscilloscope measurements, set vertical scale to $20mV$, adjust trigger to $10mV$, and take a range of frequency values and average

• Baseline snapshot

- 1500 snapshot
- 1700 snapshot
- 1500 rate of events
- Feed the anode signal with source into the Linear FiFo; one output going to the discriminator with a threshold of $10mV$ and output directly to a visual scalar. The second output should go to the oscilloscope.
 - For scalar measurements, remove the VETO for 100 seconds and record the count on the scalar
 - For Oscilloscope measurements, set vertical scale to $20mV$, adjust trigger to $10mV$, and take a range of frequency values and average
- 1500 dark current
 - Feed the anode signal into the Linear FiFo; one output going to the discriminator with a threshold of $10mV$ and output directly to a visual scalar. The second output should go to the oscilloscope.
 - For scalar measurements, remove the VETO for 100 seconds and record the count on the scalar
 - For Oscilloscope measurements, set vertical scale to $20mV$, adjust trigger to $10mV$, and take a range of frequency values and average

• Rise time

- Plug into oscilloscope and read off the numbers

- Note: All measurements using the splitter or attenuators will result in values that are one half (for the splitter) or a fraction of (variable based on the attenuator) their actual value
- Add test results and notes to corresponding database entry. All measurements should have corresponding Oscilloscope snapshots and histograms where applicable.
- Remove any grease from black box at end of day.

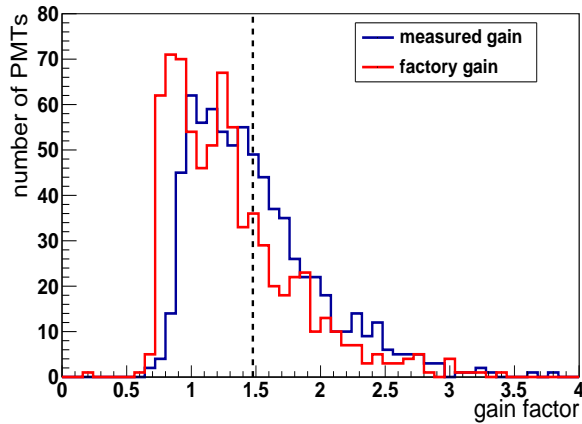


Figure 41: gain

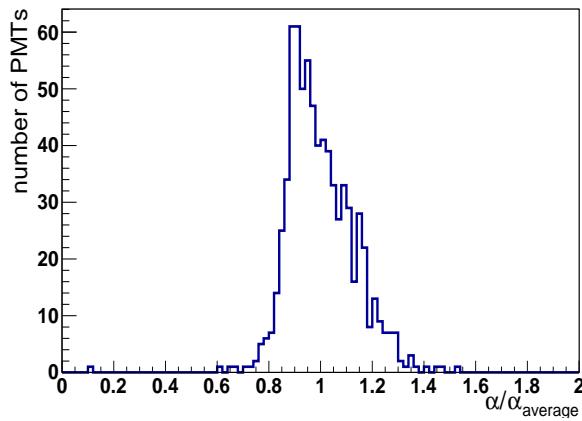


Figure 42: alpha

Counter Assembly

- Crew size: 2-3, depending on length.
- Prepare and clean workbench area, and retrieve six identical-length scintillators from storage area.
- Use latex gloves before further handling the scintillators.
- Grease and oils from hand have different reflective properties creating anomalies in further measurements? Can oils ruin scintillators? Could this be included in warnings section at top?

- Remove protective film only at the end faces of the scintillators.
- Each end of the scintillator is fitted with black tape (hereon referred to as “anticookie”), which masks the corners while leaving a circular window that extends one millimeter into the area that will be covered by the PMT. Apply anticookie end window.
- Mask the scintillator around top edges of protective tape with electrical tape slightly above the top edge. Fold the tape down to prevent glue dripping.
- Place the scintillators Diamond cut side facing you horizontally into the windmill frame while maintaining a balanced load.
- Pressurize the air pistons to 40 psi to secure the scintillators in place.
- Use the hydraulic lift to raise the windmill frame, clearing it for rotation, and rotate so that the scintillators are vertically aligned.
- Secure height and rotation angle, and keep the compressor powered.
- Mount centering tool with open side facing you. Leave a 1.5 cm gap between the top of the scintillator and the centering tool for easy centering.
- Extract 7.4 ml of each of scintillator glue and 2.4 ml of catalyst using disposable syringes and squirt the content into a disposable mixing container.
- Mix and pour glue into a capped syringe with its stopper removed and mount it into one of the base holes in the vacuum chamber and seal.
- Close all valves and open valve to chamber from pump. Evacuate chamber to 30 psi. Close valve, turn pump off, and wait for 2 minutes. Open release valve on pump farthest from chamber to protect pump from condensation. Open release valve on chamber to restore pressure, and wait 2 minutes. Close all valves.
- Wrap paper towel around bottom base of centering to catch excess glue.
- Prepare PMT for gluing.
- Place stopper in syringe and squeeze out any remaining air from tip.
- Apply approximately 1ml of glue to the top end of a scintillator, straight down in the center of the anticookie.
- Check for bubbles in glue. If bubbles are found reapply glue.
- Lower the PMT in a rotating motion through the centering tools slowly onto the scintillators ensuring that copper on PMT points to front left corner.
- Continue process until all PMT’s are mounted checking the syringe for any glue bubbles near the tip. If glue bubbles are present in the syringe you must remix new glue to ensure there are no bubbles.
- Using an Allen wrench set width of centering tools to center PMT if needed.
- Look in open area of centering tool to make sure the PMT is centered, then center between diamond-tooled side with gloved fingers. Re-verify centering of molded side with eyes.

- Distribute 3 wires evenly about PMT.
- After at least 12 hrs, rotate the windmill frame with the scintillators by 180° , and repeat the gluing process.
- After at least 12 hrs, rotate the windmill frame into the horizontal, turn off the air compressor, and release the pressure.
- Prepare and clean workbench area, and move one counter onto the workbench.
- Create a single counter label that includes the manufacturer-provided identification numbers for the scintillator and the PMT's, as well as a position dependent number i from 1, most inner and shortest, to 64, most outer and longest scintillator.
- Check that PMT orientations align with each other.
- If the PMT's do not align with each other they must be re-glued.
- If the PMT's align with each other but are offset from center you may continue.
- File the corners of the diamond cut ledge to further protect wrapping.
- File the corners smooth with a fine file.
- Blow scintillator with compressed air to remove dust.
- Remove black electric tape from ends of scintillator.
- Remove protective film, keep track of the new counter label, and remember that you will not be able to attach the new label until the entire wrapping procedure is concluded.
- Perform detailed scintillator visual inspection, and record all inclusions, bubbles, scratches, cloudy areas, refraction index changes, or any other anomalies with their respective sizes and coordinates.
- Identify diamond-tool-finished (defining the height) and molded (defining the width) sides. The molded side should be face up and defines the front of the scintillator.
- For previously non-centered but aligned PMT pairs it will be important to orientate the bar such that the side with the greatest gap between the PMT and the edge of the bar be face up denoting the front of the scintillator.
- File corner edges of scintillators to protect light tight wrapping. Using a flat coarse file file the corner down $4mm$; Only file away from the anticoke during this step.
- Log progress in check sheet.
- Cut the Mylar film to length, and wrap the counter in a single layer. Apply the transparent tape only on one molded side, which so defines the front side.

- Trim the Mylar film to the length of the scintillator.
- Cut the Tedlar film in half with the spool-mounted cutting tool.
- Cut the Tedlar film to length (scintillator length plus $20cm$ on each end), and wrap the counter tightly and wrinkle-free in three layers. Retain the film tension with electrical tape, secured only

on the front side. Finish it off with a layer of the 5cm wide, thin, black tape running the full length of the Tedlar sheet.

- Apply the counter label to the center of the front side and cover with evenly cut clear tape.
- Record width and height every 20cm and the overall length and straightness. Verify whether they are within specifications. Add inspection notes and measurements to corresponding scintillator database entry.
- Wrap 2 layers of electrical tape around PMT 3cm from edge of scintillator and at end near wires.
- Firmly pigtail the Tedlar film as close as reasonably possible to the PMT HV divider in the center with the electrical tape, trim the Tedlar to 3cm from the PMT HV divider, and finish the pigtail by wrapping the electrical tape around the bundled Tedlar and cables extending to 5cm beyond the PMT HV divider. • Check that the ends closest to the PMT of the Tedlar pigtail are less than 15.5mm in diameter.
- Zip tie wires tightly using pliers at base of PMT and trim excess.
- Blow work area clear before starting new bar.
- Before loading the first bar into the six-bar testing rack, ensure that the previous counter control measurement has been signed off. If the rack is still loaded, stop the measurement, turn off the individual HV channels, unplug the HV, anode, and dynode cables, and unload the six-bar rack, storing each counter on the designated shelf in the storage area.
- Load the counter into the six-bar testing rack with the bottom side facing the wall.
- Add the new counter in the database by associating the entries of the two PMT's with that of the scintillator.
- Repeat the inspection and wrapping procedure for the remaining scintillators.

Counter Control Measurements

- Ensure that the six counters are properly aligned and secured in the six-bar rack.
- Connect HV, anode, and dynode cables, each set from top-left, labeled 1 to bottom-right, labeled 12.
- Apply baseline voltages according to PMT testing task database entries.
- Verify that the anode and dynode signals on the oscilloscope match the nominal documented pulse-shape distribution.
- Verify that the dark current is independent of light on/off status.
- Start LabVIEW VI “Calibration Stack Reader.vi” to begin Calibration run.
- Start LabVIEW VI “Histogram Grapher.vi”. Check that channels match PMT's on the first tab labeled Data map and press confirmation button.
- Move to the ADC tab and plot histograms by holding down the “Plot ADC DATA” button. Adjust voltage till histograms leading edge lines up with read line on all graphs. Restart both programs between each run.

- Move to TDC tab and check for consistency between each channel. If not consult task expert.
- Further help is available by pushing the Instructions button in the lower left corner of program or ask the task expert if any discrepancies remain.
- Close previous VIs and Start the LabVIEW VI “24 hour ComboStackReader.splitter.noproc.vi” to start a 24 hour run. First create a file name specific to your current task by pressing the “Enter File Name” button then hit start.
- Enter your name on screen.
- Enter your name and start time in the log book at the computer station.
- The program will run for 24 hours then create a new file every subsequent day automatically until stopped. A green light will turn on when the first 24 hours has passed. The automated analysis system will automatically process the collected data and store the results and histograms into the database when the run is complete.

Counter Control Analysis and Sign-off

- Verify that the automated analysis process is complete and that the corresponding files and database entries are present.
- Verify control histograms and spot-check database entries according to interactive checklist application, as described in more detail in Section f, Quality Assurance Plan, of this document.
- At the end of the interactive checklist, the application will request sign off and will store all responses with the user’s id.
- If sign off is not warranted, the task expert must be consulted for resolution. Backing Structure and Two-Counter Assembly
- Prepare and clean workbench area, and retrieve an odd-i backing structure
- Consult database and diagram to find corresponding counters, i and $i + 1$.
- Retrieve a pair of both the left and right stoppers, 16 screws, and, if required by the assembly plan, 4 mu-metal shields.
- Add a new two-counter assembly to the database by associating these two counters and this backing structure.
- Mount left stoppers for sectors 3, 4, and 5 in their most outward positions and for sectors 1, 2, and 6 with screws slit-centered.
- Mount right stoppers for sectors 1, 2, and 6 in their most outward positions and for sectors 3, 4, and 5 with screws slit-centered.

Backing Structure

- Prepare the backing structure for taping by first marking the placement for taping onto the struc-

ture itself. Refer to the overall diagram for the taping pattern for the current backing structure. The tape-loop pairs are at intervals of 40cm for long counters and 20cm for short counters (30cm gap between tape loop pairs). Mark additional single loops at each end following the pattern on Fig. 43.

- Apply the single-sided rubber tape to the front of the backing structure in the 30cm gap be-

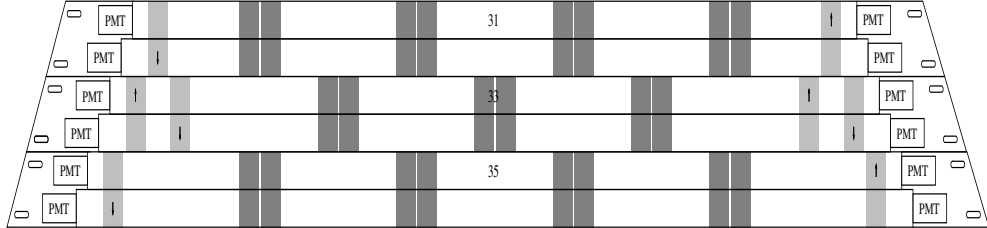


Figure 43: Final taping structure of all sectors

tween the tape-loop pair markings. The rubber tape should be measured out to 29cm and placed directly between tape-loop pairs with a half cm tolerance to the loop pairs.

- Suspend the backing structure between 2 stools/sawhorses and clamp it to them. This will allow you to freely tape the structure.
- Prepare tape-loop pairs, starting from the center of the backing structure. Tape loops of adjacent backing structures must be offset to avoid overlap, so backing structures 1, 5, 9, ... must have tape-loop pairs starting at the center, and 3, 7, 11, ... must have two central tape-loop pairs equidistant from the center (15cm). Place the tape-loop pairs in the areas previously marked for them. Each long (short) pair consists of two $5\text{cm} \times 65\text{cm}$ ($2.5\text{cm} \times 65\text{cm}$) bi-directional, double-sided fiberglass tape loops, running side-by-side extending from the back corner along the back, the side, and then across the top surfaces in opposite directions, the remaining length should overhang in preparation for the two counter pairs, as diagrammed on Fig.12, and displayed in the work area.
- An additional single tape loop must be added to the far ends of each backing structure. The loop orientation (left-handed or right-handed) will depend on the large full diagram.
- Place the longer counter onto the backing structure and orient it into its proper position. Lay the smaller counter next to it and mark its proper position onto the larger counter. This will act as a guide when taping them together.
- Caution: Tape is extremely adhesive and must be handled with care, and placed accurately. Apply the double-sided, high-tack polyester film tape along the length of the top diamond-tool-finished scintillator side of the shorter, lower, odd-numbered counter, remove the tape's protective film, and center and attach the bottom diamond-tool-finished scintillator side of the longer, upper, even numbered counter using the marks as a guide.
- Remove the protective film of the tape loops.
- Place the two-counter unit onto the backing structure, ensuring that it is positioned so that the

edge of each counter's scintillator is $1mm$ from the stoppers that have slit-centered screws.

- Continue by tightly wrapping each tape loop's remaining length around the two counter unit and back under the backing structure, completely overlapping with the first segment of the tape loop. Work as a team simultaneously on opposing tape-loop pair sides to avoid Tedlar wrinkles, especially on the top and bottom diamond-tool-finished sides, which will be stacked.
- Finish each tape-loop pair by applying a $12.7x53cm^2$ single-sided, red Mylar tape loop, with both ends terminating on the back of the backing structure, to over the double-sided fiberglass tape.
- Ensure that the slit-centered stoppers are placed and secured at $1mm$ from the scintillator end faces, and re-position the most outward-mounted stoppers at $5mm$ from the opposite scintillator end faces.
- Store the backing structure counter assembly in the designated storage area.

12.1. Quality control and tracking S/W – database and web tracking application

The results of all measurements and calculations were stored in the database. Database itself represents the set of SQL tables with web interface written on PHP. Flow-chart of the database is shown on Fig. 44.

The main table named "6 bar set" is shown by the box one on Fig. 44. This table contains the set number and length of the bars in the set which are inputted manually. All other fields in this table are filled out automatically after uploading files shown in the boxes two, three and four. These files are archive outputs of analysis programs that are described in Sect. 12.2.

As it mentioned above each set consists of six individual counters. Properties of the counters stored in the database are shown in box six. First two fields in box six ("bar number on label" and "bars number in order") are filled out manually, while last two fields are filled out automatically from uploaded archive file (box three).

Each counter in its turn consists of one scintillator and two PMTs. Properties of scintillator are stored in two tables (boxes seven and eight on Fig. 44). These tables were filled out manually by workers during the construction process. Boxes nine and ten contain properties of left and right PMTs correspondingly and are filled out manually. One more quantity that is calculated in the analysis is attenuation length, it is stored in the table (see box five) that is filled out automatically when files shown in boxes two and four were uploaded into the database. Attenuation length is the property of the scintillation material, but since PMTs are used for measurements, it's slightly different for left and right PMTs.

Besides there is one more table (box eleven) with PMTs properties that were measured before PMTs were glued to the scintillator bar. These properties (dark current, maximum magnetic field that does not distort signal, snapshots of the signals from oscilloscope etc.) were stored in excel table and graphic files and were sorted by PMTs serial numbers. Table shown by box eleven was filled out automatically when that files were uploaded. This table is linked by PMTs serial number with tables shown by boxes nine and ten, so when tables in box nine and ten are filled out the content of the table in box eleven is automatically available.

When all information about given six bar set is loaded into database one is able to print labels that should be sticked to the counter. This database is also a good tool for preliminary analysis of obtained data. For instance it allows to easily produce various plots such as time resolution versus bar length or ability to distinguish particles as function of their momentum.

12.2. Automated six-bar analysis software

Note: note: study of required number of positional measurements at <https://clasweb.jlab.org/wiki/index.php>.

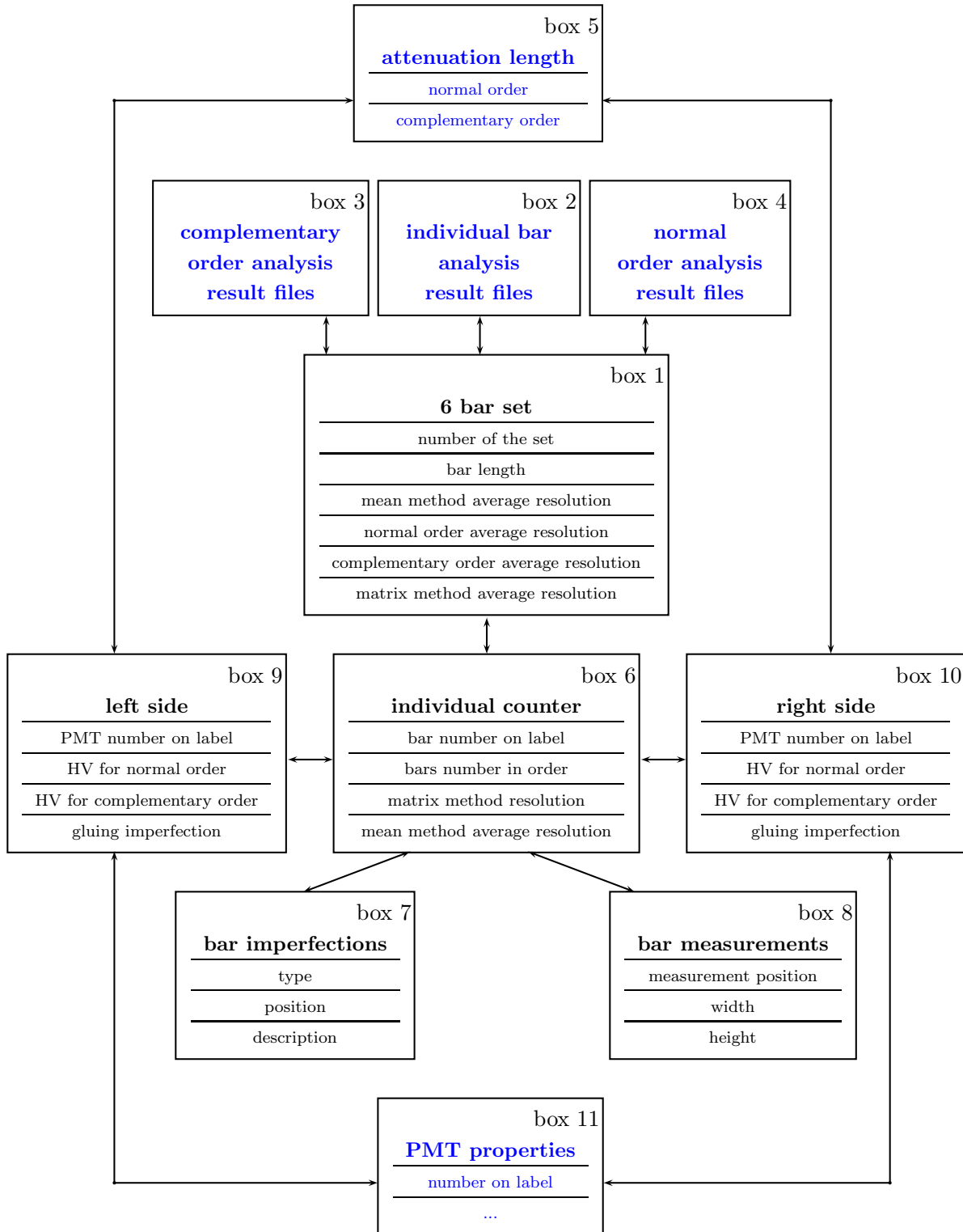


Figure 44: Database structure

For simplification the analysis procedure was splitted into several stages. For the first stage converter that transforms stored data into standart root file was developed. Root file contains root tree with variables that correspond to signals from ADCs and TDCs. This approach allows in case of using different modules (for instance we used QDC, while at JLab flash ADC will be used) to modify only the converter and keep remaining analysis software unchanged.

The reason for automated software development is the need to repeat a lot of similar computations many times. Since the time-walk corrections are position dependent all procedures described above need to be performed in each bin along the scintillator bar. In order to determine the best bin width time resolutions were compared with expected value for various numbers of bins along the bar (see Figs.). It turned out that the optimal width of the bin is around three cm. That means that number of bins varies from five for the shortest bars to 135 for the longest bars.

So-called main program uses as an input root files obtained as an output of the converter. This program performs time-walk corrections (see Sect. 3.5) and computes resolutions for each combinations of the three bars (see Sect. ??). Besides it calculates attenuation lengths and effective speeds of light (see Sect. 12.2.2). As outputs program produces two files: one file with histograms that easily can be viewed by root and another archive file that can be uploaded into and processed by database (see Sect. 12.1). Main program need to be run twice for normal and complementary orders of the bars (see Sect. ??).

Finally two output root files (for normal and complementary orders) from the main program are used as inputs for the routine that computes resolutions of individual bars. This routine solves the system of linear equations mentioned in Sect. ?. As an output again routine has two files: root and archive which can be processed by database (Sect. 12.1).

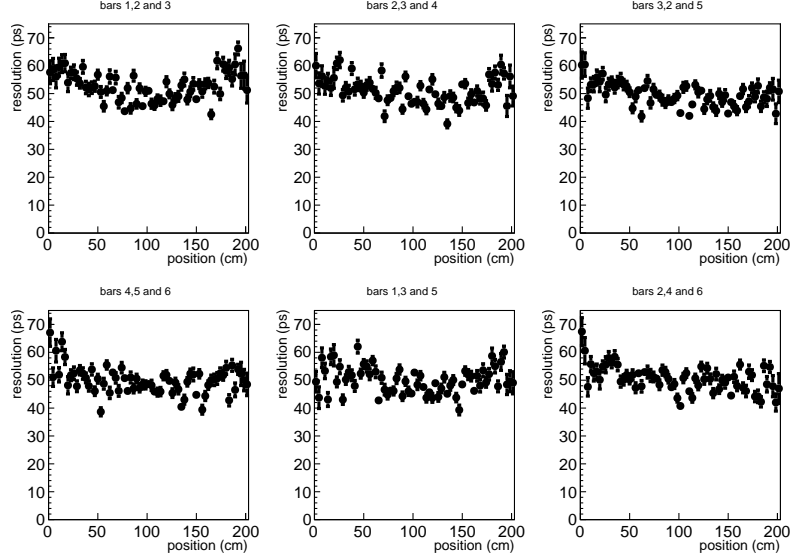


Figure 45: Time resolutions as function of position along the bar for 200 cm long bars from the set 30. Various plots represent various bars combinations

12.2.1. Time resolution

As mentioned above six-bar method (see Sect. ??) implies that six counters are put on top of each other. Since six-bar method demands multiple use of three-bar method different combinations of the counters are selected as it shown on Fig. ???. Then according to the formula ?? quantity T for each bin from Fig. 19 and for each selected three-bar combination is calculated using time-walk corrected times (see Sect. 3.5). T -distributions are plotted and fitted by gaussian. Since all counters are treated identically the formula ?? can be written in this way:

$$\sigma_{avg} = \sqrt{\frac{2}{3}}\sigma_T \quad (12.1)$$

where σ_T - spread of T -distributions and σ_{avg} - resolution averaged over given three-bar combination.

On Fig. 45 the resolutions averaged over various three-bar combinations are plotted as function of the bar length. It can be noticed that resolution in the center of the bars is higher than at the edges. This happens because the combined time-walk effect has greater impact on the edges rather than in the middle. The average values of combined resolutions are shown on Fig. 46 for each three-bar combinations. Then the same procedure is performed for so-called complementary order. Permutations of the bars are shown on Fig. ???. Calculated values of average time resolution for normal and complimentary order of bar combinations are used as an input for system of linear equations ?? in order to extract individual resolutions of each counter as described in Sec. ??.

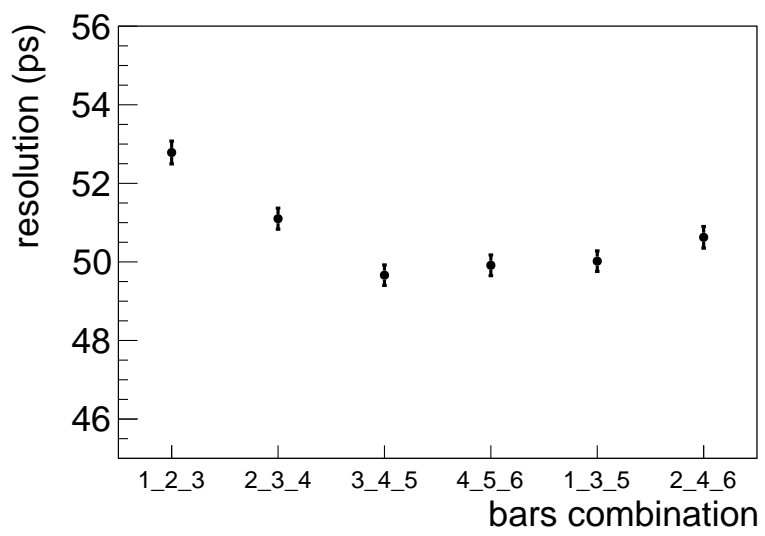


Figure 46: Average time resolutions for various combinations of the bars. Plot corresponds to the 200 cm long bars from the set 30.

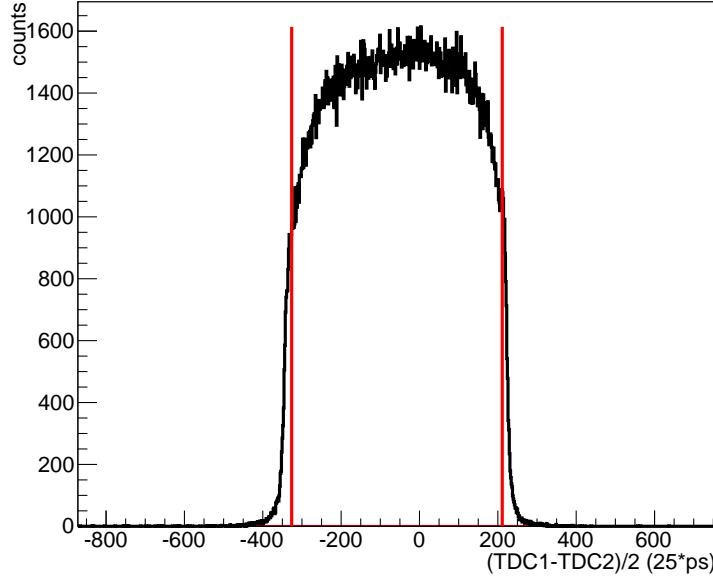


Figure 47: Half of the time-walk corrected TDC difference for the bar 200 cm long from the set 30. Vertical red lines correspond to the x -positions of half maxima for left and right slopes of the distribution.

12.2.2. Attenuation length and effective speed of light

The scintillator material for the TOF system must have short decay times, long attenuation length, and good spectral match to the PMTs. Initial measurements show that attenuation length values vary even among scintillation bars of the same material and from the same mold, so in order to verify that each counter meets required specifications, the attenuation length measurement is incorporated into the unit testing of each counter constructed for Panel 1B. The method uses the same data collected in the six-bar time resolution measurements described in Sec. ??.

Firstly the whole bar length was divided into slices by using time-walk corrected TDC difference between left and right PMTs shown on Fig. 47. Red lines on Fig. 47 correspond to the x -positions of half maxima for left and right slopes of the distribution. The distance between these lines is proportional to the bar length, so after the TDC difference was divided into slices the bar length is also automatically sliced.

For events inside each slice ADC distributions for each PMT were plotted as shown on Fig. 48. The maximum of each distribution can be determined by two methods. In the first method the position of the maximum can be found either by fitting with Landau or Gauss-convoluted Landau functions as it shown on the left side of Fig. 48. Both functions give relatively the same positions of the maximum, but Gauss-convoluted Landau fit describes data better. In the second method the center of the maximum bin of the histogram smoothed by running mean procedure is treated as the maximum of the ADC distribution as shown on the right side of the Fig. 48. Dashed vertical

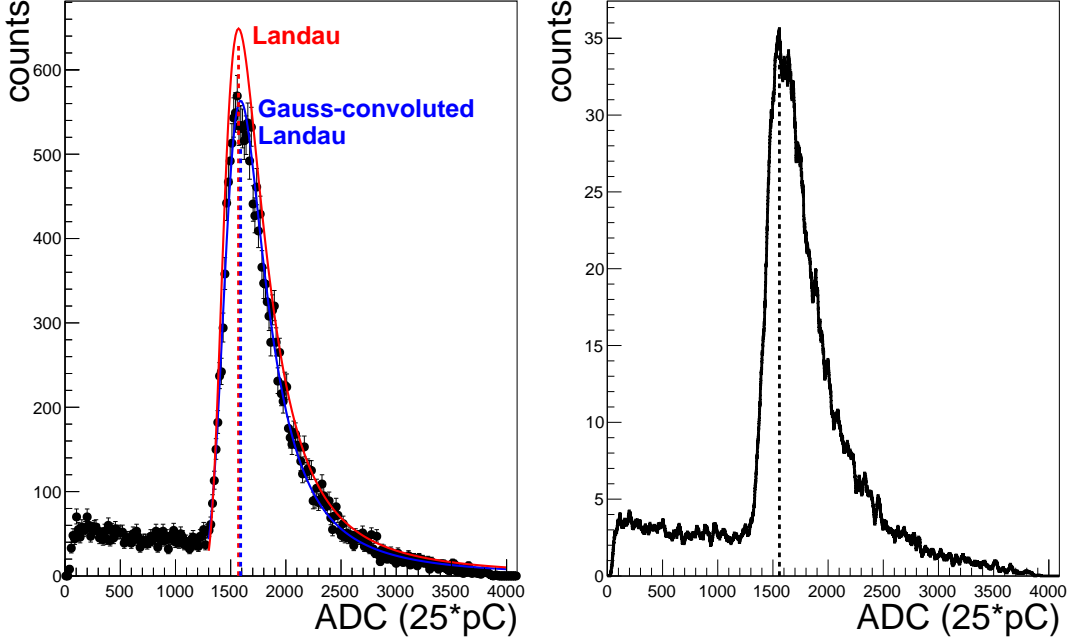


Figure 48: ADC distribution for one of the TDC difference slice from the Fig. 47 for one of the PMTs. Left side: Landau fit in comparison with Gauss-convoluted Landau fit. Since 12 bits ADCs was used the histogram had 4096 bins, for illustrative purposes each 16 bins were averaged into one. Dashed vertical lines correspond to the maximum of the distribution given bu the fits. Right side: The same ADC distribution smoothed with by running mean procedure with averaging parameter 30. Dashed vertical line represents the center of the maximum bin.

lines on both plots on Fig. 48 represent peak positions, which are relatively the same for both methods. But since the second method consumes less CPU time it was chosen as preferable to analyze the rest of the data.

Then obtained maxima positions were plotted versus position along the scintillator length Fig. 49. Attenuation length was determined by fitting this distribution with convolution of two exponents (12.2).

$$N = N_0^T e^{-x/\lambda_T} + N_0^B e^{-x/\lambda_B}, \quad (12.2)$$

where $N_0 = N_0^T + N_0^B$ is the initial number of photons caused by the cosmic ray passing through the scintillator at the impact position x and N is the number of photons arriving at the PMT. Since attenuation length of scintillator can be divided into two parts two exponential functions were used for the fit. One part is called the technical attenuation length (TAL), which is defined as the length reducing the amount of light by a factor e and depends on the geometry of the scintillator and the reflective properties of its surface. The other part is called bulk attenuation length (BAL), which reduces the initial light intensity by a factor e according to the Buger-Lambert Law and depends on the transparency and the scintillation material.

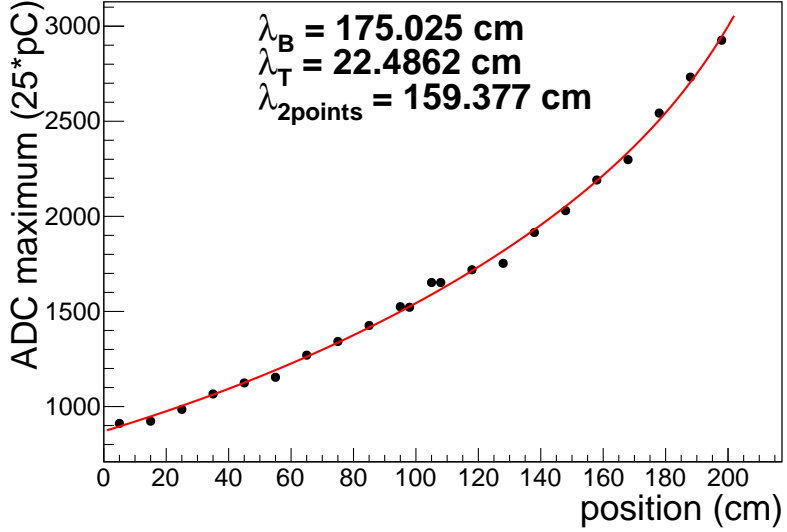


Figure 49: Maxima positions of the ADC distributions for one of the PMTs as function of position along the scintillator bar. Red curve represents fit by two exponential function from Eq. 12.2. λ_B and λ_T are bulk and technical attenuation lengths correspondingly, which were determined from the fit. $\lambda_{2points}$ is bulk attenuation length determined from two penultimate points.

In addition to the exponential fit attenuation length was also determined by the two points method, where technical attenuation length is treated as negligible (12.3). For that purpose x and y coordinates of penultimate points from each side of distribution like Fig. 49 were inserted into equation 12.3 instead of x and N correspondingly. After that obtained system of two equations was solved for $\lambda_{2points}$.

$$N = N_0 e^{-x/\lambda_{2points}}, \quad (12.3)$$

Results for attenuation length obtained from left and right PMT for each bar are almost the same, so finally the averaged value was taken. On Fig. 50 bulk attenuation length is plotted as function of the set number. Various symbols correspond to different scintillators in the set. The gap at set number 32 corresponds to the fact that according to design requirements for short counters, less than 200 cm in length, fast material with short attenuation length is needed, while for long counters scintillators with large attenuation length is the better choice.

To determine effective speed of light for each scintillator the ratio of bar length, which is known, over the light passing time, which is extracted from TDC values is taken. Light passing time is determined by the distance between red lines on the Fig. 47. Effective speed of light for six scintillators from one set is shown on Fig. 51. It could be noticed that effective speed of light appears to be slightly higher for bars closest to the center in the six-bar set. This effect can be explained in the following way. Only those tracks that hit all six bars are taken into account, but

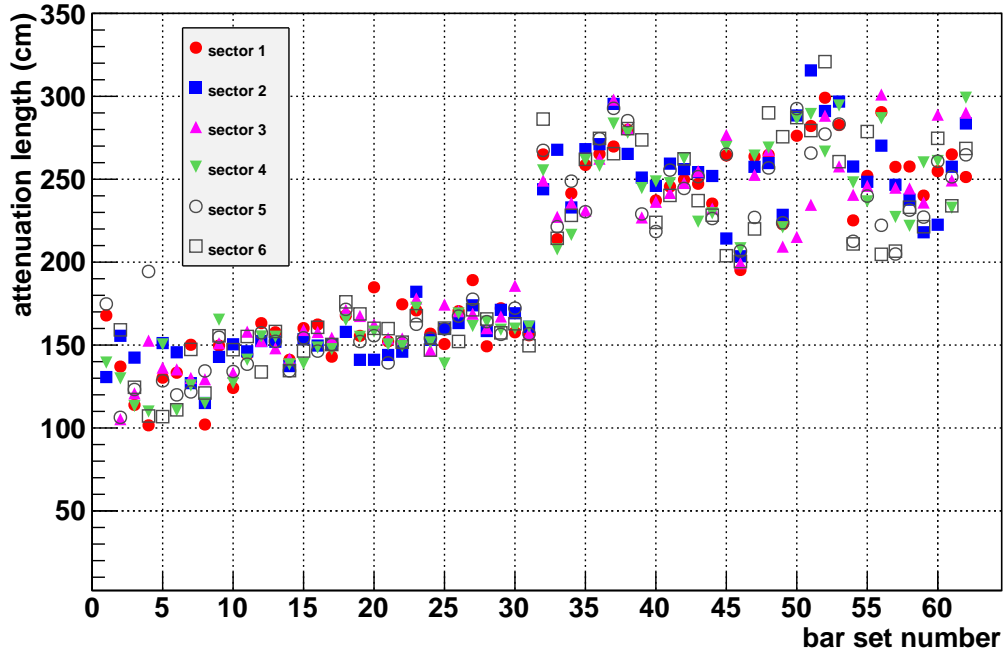


Figure 50: Averaged bulk attenuation length versus set number. Various symbols correspond to the different scintillators in the set or in other words to CLAS12 sectors.

the behaviour of non-vertical tracks differs from the vertical. Vertical track hits all bars in the set at the same position, but non-vertical track, which hits edges of the top and bottom bars, hits other bars farther from the edges. So, the closer bar to the center of the set the less tracks hit the edges of the bar and the more narrow TDC distribution appears to be.

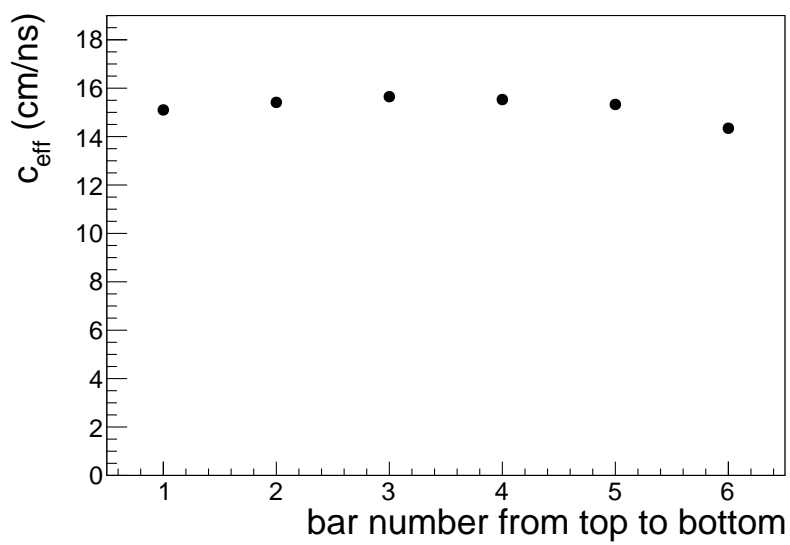


Figure 51: Effective speed of light as function of bar number in the set. Example is given for set number 30.

13. Results and Summary

The technique that allow to extract individual bar resolution using cosmic rays was developed. Resolutions obtained in our measurements exceed JLab requirements. By now the world best resolution for given scintillator length was achieved.

References

- [1] E. S. Smith, et al., The time-of-flight system for CLAS, Nucl. Instrum. Meth. A432 (1999) 265–298. doi:10.1016/S0168-9002(99)00484-2.
- [2] CLAS12 Technical Design Report v5.0 (July 2008).
- [3] V. Batourine, W. Kim, D. Nekrasov, K. Park, B. Shin, E. Smith, S. Stepanyan, CLAS-NOTE-2004-016: Measurement of PMT Time Resolution at Kyungpook National University (2004).
- [4] Caen, Mod. V1290-VX1290 A/N, 32/16 Ch. Multihit TDC (June 2009).
- [5] Caen, Mod. V792/V792N 32/16 channel QDC (May 2009).
- [6] W. Leo, Techniques for Nuclear and Particle Physics Experiments: A How to Approach, Berlin, Germany: Springer, 1987.
- [7] R. S. Ralf Gothe, Evan Phelps, Y. Tian, Ftof12 forward time-of-flight at usc: A comprehensive update, ftof12 technical system review, jefferson lab, newport news, va (2009).